Journal Pre-proof

Satellite synergy: Navigating resource allocation and energy efficiency in IoT networks

Muhammad Abdullah, Humayun Zubair Khan, Umair Fakhar, Ahmad Naeem Akhtar, Shuja Ansari

PII: S1084-8045(24)00143-7
DOI: https://doi.org/10.1016/j.jnca.2024.103966
Reference: YJNCA 103966

To appear in: *Journal of Network and Computer Applications*

Received date : 17 August 2023
Revised date : 19 May 2024
Accepted date : 26 June 2024

Please cite this article as: M. Abdullah, H.Z. Khan, U. Fakhar et al., Satellite synergy: Navigating resource allocation and energy efficiency in IoT networks. *Journal of Network and Computer Applications* (2024), doi: https://doi.org/10.1016/j.jnca.2024.103966.

Satellite Synergy: Navigating Resource Allocation and Energy Efficiency in IoT Networks

Muhammad Abdullah[1], Humayun Zubair Khan[1,2], Umair Fakhar[1], Ahmad Naeem Akhtar[3], and Shuja Ansari[2]
[1] National University of Sciences and Technology, Islamabad 44000, Pakistan
[2]University of Glasgow, Glasgow 12G8QQ, United Kingdom
[3]Lahore Garrison University, Lahore 54792, Pakistan
Corresponding E-mail:humayunkhan@mcs.edu.pk

***Abstract*—Satellite-assisted internet of things (IoT) networks have emerged as a beacon of promise, offering global coverage and uninterrupted connectivity. However, the challenges of resource allocation and task offloading in such networks are intricate due to the unique characteristics of satellite communication systems. This research's findings enrich the landscape of energy-efficient and dependable satellite-assisted IoT networks. The paper navigates the delicate balance between energy efficiency, network throughput, and fairness in distributing resources among IoT devices. The proposed techniques, notably the Outer Approximation Algorithm (OAA), usher in seamless connectivity and resource optimization. The central challenge at hand, a concave fractional programming problem, transforms through the Charnes-Cooper transformation, presenting as a concave optimization enigma. Herein, the proposed outer approximation algorithm takes flight, navigating the intricate paths of concave optimization. The performance of the epsilon-optimal solution faces scrutiny under diverse system parameters—the constellation of IoT devices, their affiliations, fairness considerations, and the equitable distribution of resource blocks. This contribution not only enriches research but also opens doors to the boundless possibilities of satellite-assisted IoT networks.**

***Index Terms*—IoT association, task offloading, resource allocation, MINLP, satellites**

I. Introduction

In the contemporary landscape, IoT devices seamlessly intertwine with our daily lives, signifying their integral role [1]–[3]. Advancements in intelligent technologies and applications continue to unfold, ushering in an era of growing benefits. Notably, the energy consumption of persistently operational apps, fueled by transmitted data, exceeds that of their non-intelligent counterparts, offering a glimpse into the intricate balance between innovation and resource expenditure. Cloud computing has emerged as a versatile player, influencing a range of scenarios—from cloud radio access networks (C-RANs) to intricate heterogeneous networks (HetNets), vehicle ad hoc networks (VANETs), and vibrant social networks [4]–[6].

These strides transform communication and bring forth intriguing inquiries. Within this symphony of technology, the pursuit of energy efficiency emerges as a guiding star, converging with the surge of interconnected IoT devices [7]–[9]. This endeavor stems from the urgency to optimize network assets and curtail energy consumption, fostering sustainability [10]. In response to scientific proposals, the board aims to illuminate energy consumption and real-time communication. While centralizing data within cloud servers offers benefits, it brings inherent drawbacks. Escalating traffic, prolonged processing, intensified energy needs, and mounting costs underscore the intricate orchestration, especially in fifth-generation networks [11], [12].

Present satellite-based communication divides into three: Geosynchronous Earth Orbit (GEO), Medium Earth Orbit (MEO), and Low Earth Orbit (LEO) [13]. The future integrates satellite and terrestrial networks, heavily relying on Low Earth Orbit (LEO) satellites for minimal latency. Integration is poised for next-gen wireless networks, particularly 5G, promising widespread high-speed Internet access [14]. Urban IoT networks leverage 3G, 4G, or 5G for data collection. Coupling Low Earth Orbit (LEO) satellites with global access networks extends potential for distributed IoT networks. Yet, IoT gateways reliant on low-Earth orbit satellites encounter data caching hurdles [15]. This landscape underscores infrastructure's pivotal role in IoT's growth.

Wireless networks shift with IoT's global adoption, intensifying traffic demands [16]. The pursuit culminates in equitable high-speed Internet access transcending boundaries [17]. Despite terrestrial advancements, rural areas face limited terrestrial backhaul network reach [18]. Energy efficiency becomes paramount in IoT's interconnectivity. Green fog computing offers solutions for latency-sensitive IoT applications. But, solutions require innovative resource allocation and network modeling, balancing power, energy, cost, and latency [19].

This paper embarks on enhancing cache availability, expanding storage on fog nodes, and optimizing energy efficiency. Integration with GEO/LEO satellites takes center stage, aiming to create a fairness-aware planning framework. This framework harmonizes elements like association control, transmission power, and bandwidth allocation to minimize IoT device task delays. As we embark, a consistent terminology shall be our compass.

A. *Related work*

The literature review [20]- [32] explores satellite-based IoT network studies, addressing connectivity challenges and proposing solutions. While these studies delve into various aspects, they often overlook fairness in IoT distribution and data access delays. Bridging this gap is essential for a comprehensive understanding of IoT networks' capabilities and

TABLE I
RELATED WORK AND NOVELTY

Parameters	[20] **2021**	[21] **2021**	[22] **2021**	[23] **2020**	[24] **2019**	[25] **2021**	[26] **2022**	[27] **2022**	[28] **2022**	[29] **2021**	[30] **2021**	[31] **2021**	[32] **2020**	This paper
Transmission in UL				✓	✓					✓			✓	✓
IoT Admission														✓
IoT Association	✓		✓							✓			✓	✓
Power limit	✓	✓	✓		✓	✓	✓	✓	✓	✓	✓	✓	✓	✓
Geo satellite (cloud)	✓	✓	✓								✓	✓		✓
Leo satellite (cloudlet)	✓	✓	✓							✓		✓	✓	✓
Effect of Rain														✓
Movement of Satellite														✓
Processing delay				✓			✓			✓	✓	✓	✓	✓
Transmission delay			✓	✓							✓	✓	✓	✓
Propagation delay						✓							✓	✓
Queuing delay													✓	✓
Cache enabled									✓		✓	✓	✓	✓
Data computation									✓		✓	✓		✓
Data storage									✓		✓	✓	✓	✓
Fair IoT and RBs distribution														✓
Energy efficiency	✓						✓	✓			✓	✓		✓

limitations. Table I summarizes previous work on resource allocation in S-IoT networks.

In the cited literature, several research papers have explored various aspects of satellite-based communication systems and their implications for Internet of Things (IoT) networks. [20] presented a comprehensive perspective on global connectivity challenges and introduced a 5G smart connectivity platform as a solution. This platform's automation capabilities enable effective service management, addressing these challenges with minimal costs. Satellites, unmanned aerial vehicles (UAVs), and long-range, low-power IoT network technologies have been identified as key enablers to extend 5G cellular coverage to remote and unreachable locations. [21] delved into the realm of satellite communication systems by proposing a joint beam management and power allocation strategy to enhance signal-to-interference-plus-noise ratio (SINR) and mitigate outages. To tackle the intricate problem of allocating transmit power for active low-Earth orbit (LEO) satellites, the author introduced a deep Q-network (DQN) approach, while the application of non-orthogonal multiple access (NOMA) techniques enhanced spectral efficiency. In the realm of GEO/LEO satellite networks, research by [22] formulated a theoretical approach, deriving the ergodic capacity of a two-layer network using Meijer-G functions. However, these studies primarily focused on IoT device association for satellite networks, neglecting fairness considerations and data access delays.

[23] explored cooperative user association and resource allocation strategies for hybrid GEO-LEO satellite networks, tackling the challenge of task scheduling and user association in a multi-tier framework. Similarly, [24] proposed sub-band allocation and power regulation methods for boosting IoT cellular network throughput, considering spectral leakage effects. Resource allocation challenges in quantum key distribution (QKD) networks that employ both GEO and LEO satellites were addressed by [25], introducing sub-optimal strategies for minimizing energy consumption and optimizing secret key generation. [26] focused on energy-efficient relay selection and power allocation strategies for communication networks, particularly considering load balancing within the context of relay-assisted communication. [27] proposes relay selection and power allocation to improve energy efficiency and load balancing in RLNC D2D communications supporting HetNets in reference.

[28] tackled work offloading and software cache optimization through an iterative approach, aiming to reduce task execution delays by caching frequently used services. [29] explored low-latency edge computing provided by flying unmanned aerial vehicles (UAVs) and satellite-based cloud access, with a comprehensive optimization approach considering various parameters such as association control, computing job allocation, and resource allocation for UAVs. [30] introduced constrained joint node association and energy efficiency maximization problems for IoT-Fog networks, devising suboptimal solutions for power allocation and node association using linearization strategies. Additionally, latency minimization in cloudlet-based IoT networks was tackled through an Outer Approximation Algorithm (OAA) approach [31]. In the context of fog networks, [32] addressed the intricate challenge of resource and power allocation for minimizing energy consumption while considering factors like QoS constraints, cache capacity, and network latency.

While these studies contribute significantly to satellite-based IoT networks, they commonly lack an emphasis on fairness in IoT distribution and data access delays. This research gap highlights the need to explore these dimensions for a comprehensive understanding of IoT networks' capabilities and limitations.

B. Motivation and Contributions

Reviewing the synthesis of previous endeavors [20]- [32] in Table I, our primary focus resides in the realm of resource allocation and task offloading challenges within IoT ecosystems. Specifically, we delve into scenarios where IoT devices strive to establish connections with LEO-cloudlets in the uplink direction. These devices transmit data files to LEO-cloudlets for storage and computation, further extending to offloading

requests to cloudlets. This becomes particularly relevant in expansive geographical zones, encompassing remote areas void of terrestrial access networks. In such intricate landscapes, the deployment of satellite communication systems emerges as a pivotal enabler for IoT devices, facilitating operations within these far-flung and secluded regions.

The nucleus of our research orbits around optimizing end-to-end network energy efficiency. Our objective embraces IoT device admission, association with LEO satellites, latency considerations, cache capabilities, impact of inclement weather like rain, satellite movement dynamics, and power allocation within satellite-based IoT (S-IoT) networks.

A pivotal dimension of our investigation concerns equitable assignments of IoT devices to suitable associations and impartial distribution of spectrum resources. These objectives harmoniously align with the overarching mission of enhancing energy efficiency. This distinctive objective, somewhat unexplored in prior studies, necessitates the delicate equilibrium between fairness and the quest for peak energy efficiency.

The optimization challenge at hand is intricate, characterized by the amalgamation of integer and nonlinear variables, rendering it a mixed-integer nonlinear programming (MINLP) problem. In response, we present an inventive iterative algorithm—the outer approximation (OAA). This algorithm deftly dissects the problem into discrete components, ultimately culminating in an optimal solution. Through this novel approach, we adeptly navigate the intricacies and complexities entwined with the challenge.

To assess the potency of our proposed methodology, we intend to conduct a thorough comparative analysis against existing state-of-the-art techniques. This evaluation endeavors to decipher the precise influence and contributions of our approach. Notably, the contrasts delineated in Table I underscore the discernible and substantial enhancements our method ushers in.

The noteworthy contributions of our work can be encapsulated as follows:

1) **Innovative Architecture for Resource Allocation and Task Offloading:** Our approach introduces a cutting-edge architectural framework for resource allocation and task offloading across multiple tiers, seamlessly integrating satellite support. Anchored in the concept of IoT devices collecting data from their ambient surroundings, especially in remote and underserved locales devoid of terrestrial infrastructure, our methodology brings forth an efficient task execution system.
2) **Formulation and Transformation of Complex Problem:** The complex challenge assumes the form of a concave fractional programming (CFP) problem, encompassing vital constraints such as IoT association, power allocation, latency, storage, QoS data rates, satellite movement dynamics, and more. Employing the Charnes-Cooper transformation (CCT), we adeptly transmute the CFP problem into solvable concave optimization problems.
3) **Innovative Iterative Algorithm—Outer Approximation (OAA):** Our research introduces a novel iterative algorithm, the outer approximation. Through relaxation approaches, we disentangle the challenge into non-linear and mixed-integer linear components. By navigating between upper and lower bounds, this algorithm iteratively seeks optimal solutions, skillfully addressing the inherent intricacies.
4) **Evidence through Comprehensive Simulations:** Utilizing meticulous simulations, we rigorously assess the effectiveness of our proposed Satellite-based IoT network system. The simulation results provide compelling evidence that our algorithm excels, particularly in terms of IoT association and the attained energy efficiency within the context of satellite-assisted IoT networks.

In summation, our research propels advancements in energy-efficient satellite-based IoT networks, elevating resource allocation, task offloading, and their associated complexities.

In Section II, we perform an extensive review of pertinent literature to contextualize our study within the existing body of research. Moving to Section III, we outline the system model and provide a comprehensive problem description. Our innovative solution to the identified problem is evaluated in Section IV through a dynamic framework. In Section V, we delve into the specifics of simulation variables and their corresponding outcomes. Lastly, Section VI encapsulates our study's findings and draws meaningful conclusions.

II. System Model and Problem Formulation

A. *Network model*

Figure 1 illustrates a three-tier architecture comprising IoT devices, cloudlets, and clouds. In this context, LEO and GEO satellites assume the roles of cloudlets and clouds respectively. We make the assumption that IoT devices are situated in remote or inaccessible regions where conventional telecommunication infrastructure is absent. These IoT devices are equipped with sensors to gather data from their surroundings and transmit it to third-party entities for tasks such as storage, data fusion, and computation. Given the inherent limitations of these IoT devices in terms of storage and computation capabilities, LEO and GEO satellites come equipped with ample on-board storage and computation resources. As such, the LEO satellite functions as a cloudlet, while the GEO satellite functions as a cloud, offering essential services such as storage and computation to IoT devices situated in remote areas devoid of telecommunication infrastructure.

Lets consider a system with time slots and indexed as $t \in \mathbf{T} = \{0, 1, 2, 3, ...\}$. Lets a set of IoT devices denoted by $\mathbf{I}(t)$ where $i(t) \in \mathbf{I}(t) = \{1, 2, 3, ..., I(t)\}$ are operating in the time slot t and this set of IoT devices are served when $J(t)$ number of LEO-cloudlets where $j(t) \in \mathbf{J}(t) = \{1, 2, 3, ..., J(t)\}$ fly over the $I(t)$ IoT devices in far flung area. These LEO-cloudlets are inter-connected via microwave links to share the traffic load of $I(t)$ IoT devices with fairness. Moreover, $J(t)$ LEO-cloudlets have a high capacity microwave link with the GEO-cloud. The GEO-cloud will share the work load in case the LEO-cloudlet $j(t)$ can't entertain the storage, and the computation request from a IoT device $i(t)$. Thus, there are two different modes of communication and discussed separately in sub-section II-C.

B. *Resource allocation model*

Few binary variables to show IoT device $i(t) \in \mathbf{I}(t)$ admission, association, and availability of LEO-cloudlet are defined below:

- **definition-1:** Let the 0/1 indicator to show wether a IoT device $i(t) \in \mathbf{I}(t)$ is admissible or not is given below:

$$x_i(t) = \begin{cases} 1, & \text{IoT device is admissible} \quad (1a) \\ 0, & \text{Otherwise} \quad (1b) \end{cases}$$

- **definition-2:** Let the 0/1 indicator to show wether a IoT device $i(t) \in \mathbf{I}(t)$ is associated with LEO-cloudlet $j(t) \in \mathbf{J}(t)$ or not is given below:

$$y_{i,j}(t) = \begin{cases} 1, & \text{IoT device is associated} \quad (2a) \\ 0, & \text{Otherwise} \quad (2b) \end{cases}$$

- **definition-3:** Let the 0/1 indicator to show wether a LEO-cloudlet $j(t) \in \mathbf{J}(t)$ is available to fulfill request of the IoT device $i(t)$ or not is given below:

$$z_{i,j}(t) = \begin{cases} 1, & \text{LEO-cloudlet is available} \quad (3a) \\ 0, & \text{Otherwise} \quad (3b) \end{cases}$$

In this context, it is observed that a LEO-cloudlet denoted by $j(t) \in \mathbf{J}(t)$ has the capability to offer its services to multiple IoT devices. However, an IoT device represented by $i(t) \in \mathbf{I}(t)$ is restricted to associate with only a single LEO-cloudlet, namely $j(t) \in \mathbf{J}(t)$. This association of IoT devices should be such that fairness is maintained while distributing the traffic load among all LEO-cloudlets. Mathematically, the fairness is ensured using Jain's fairness index [33] as below:

$$\alpha_{i,j}(t) = \frac{\left(\sum_{j(t)\in\mathbf{J}(t)} \left(\sum_{i(t)\in\mathbf{I}(t)} y_{i,j}(t) \right) \right)^2}{J(t) \left(\sum_{j(t)\in\mathbf{J}(t)} \left(\sum_{i(t)\in\mathbf{I}(t)} y_{i,j}(t) \right)^2 \right)}, \quad (4a)$$

$$0 \leq \alpha_{i,j} \leq 1), \quad (4b)$$

where $\alpha_{i,j}(t)$ in (4a) is the user fairness index (UFI) and it's value ranges between zero and one as shown in (4b). The value of UFI is one when the distribution/ association of $I(t)$ IoT devices traffic load to the $J(t)$ LEO-cloudlets follow the optimum fairness.

Every IoT device $i(t) \in \mathbf{I}(t)$ can transmit data file to the LEO-cloudlet $j(t) \in \mathbf{J}(t)$ using it's power within upper limit of P_i. Mathematically, the range of allocated power with in the upper limit is given below:

$$0 \leq p_{i,j}(t) \leq P_i, \ \forall\, i(t) \in \mathbf{I}(t), \ j(t) \in \mathbf{J}(t), \quad (5)$$

Every IoT device $i(t) \in \mathbf{I}(t)$ can associate and transmit data to a LEO-cloudlet $j(t) \in \mathbf{J}(t)$ [34]. The signal in the UL suffers path loss, attenuation due to rain, and attenuation due to atmospheric gasses when a IoT device $i(t) \in \mathbb{I}(t)$ associates and transmits data to LEO-cloudlet $j(t) \in \mathbf{J}(t)$. The channel

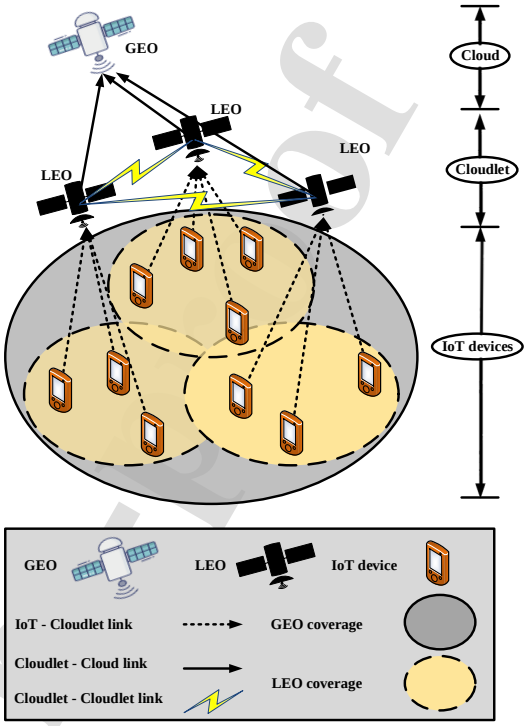

Fig. 1. **System Model - GEO and LEO hybrid satellite network**

gain between a IoT device and a LEO-cloudlet in the UL is given by [35].

$$h_{i,j}(t) = \frac{G_i^{\mathrm{Tx}} G_j^{\mathrm{Rx}}}{\xi_{i,j}^{PL}(t) \xi_{i,j}^{Rain}(t) \xi_{i,j}^{Gas}(t)}, \quad (6a)$$

$$\xi_{i,j}^{PL}(t) = \left(\frac{4\pi f_c s_{i,j}(t)}{\upsilon} \right)^2, \quad (6b)$$

$$\xi_{i,j}^{Rain}(t) = J_r \Re^{\mu_r} L_e, \quad (6c)$$

$$\xi_{i,j}^{Gas}(t) = \frac{A_w A_o}{sin\theta_{i,j}(t)}, \quad (6d)$$

where G_i^{Tx} and G_j^{Rx} are the antenna gains of the Internet-of-Things device and the low-Earth-orbit cloud node, respectively. Attenuation due to free-space path loss, rain, and atmospheric gases are denoted by $\xi_{i,j}^{PL}(t)$, $\xi_{i,j}^{Rain}(t)$, and $\xi_{i,j}^{Gas}(t)$, respectively. f_c is the carrier frequency, and $s_{i,j}(t)$ is the separation between the Internet of Things node $i(t) \in \mathbf{I}(t)$ and the low Earth orbit cloud node $j(t) \in \mathbf{J}(t)$. The υ denotes the velocity of light. The coefficients J_r and μ_r change with the frequency. The effective path length of a wave in rain is denoted by L_e, while the intensity of rainfall is denoted by $\Re$. A_w and A_o are the absorptions due to water vapours and oxygen, respectively [36]. $\theta_{i,j}(t)$ is the elevation angle between IoT device $i(t) \in \mathbf{I}(t)$ and LEO-cloudlet $j(t) \in \mathbf{J}(t)$ [37].

attainable uplink data rate $\psi_{i,j}(t)$ from IoT device $i(t) \in \mathbf{I}(t)$ to the LEO-cloudlet $j(t) \in \mathbf{J}(t)$ is calculated as follows, in accordance with shannon's capacity theorem:

$$\psi_{i,j}(t) = b_{i,j}(t) log_2\left(1 + \Phi_{i,j}(t)\right), \tag{7a}$$

$$\Phi_{i,j}(t) = \frac{p_{i,j}(t) h_{i,j}(t)}{I_{i',j}(t) + \sigma^2}, \tag{7b}$$

$$I_{i',j}(t) = \sum_{j(t)\in\mathbf{J}(t)} y_{i',j}(t) p_{i',j}(t) h_{i',j}(t), \tag{7c}$$

where $i' \neq i$, $y_{i,j}(t) = 1$ when IoT device $i(t) \in \mathbf{I}(t)$ associates with the LEO-cloudlet $j(t) \in \mathbf{J}(t)$, and $y_{i,j}(t) = 0$ otherwise. The channel bandwidth is denoted by $b_{i,j}(t)$, while the signal to interference and noise ratio is represented by $\Phi_{i,j}(t)$. The noise is denoted by σ^2, and the interference from IoT device $i'(t) \in \mathbf{I}(t)$ to LEO-cloudlet $j(t) \in \mathbf{J}(t)$ in the UL is represented by $I_{i',j}(t)$. The resource blocks are allocated to a IoT device $i(t) \in \mathbf{I}(t)$ by LEO-cloudlet $j(t) \in \mathbf{J}(t)$ as per the requirement of quality of service (QoS). For a given data rate QoS and resource block fairness index (RFI), the following mathematical expressions can be used to determine the necessary number of resource blocks:

$$r_{i,j}(t) = \left\lceil \frac{Q_{i,j}(t)}{\psi_{i,j}(t)} \right\rceil, \tag{8a}$$

$$\gamma_{i,j}(t) = \frac{\sum_{j(t)\in\mathbf{J}(t)} r_{i,j}(t)}{\sum_{j(t)\in\mathbf{J}(t)} y_{i,j}(t)}, \tag{8b}$$

$$\beta_{i,j}(t) = \frac{\left(\sum_{j(t)\in\mathbf{J}(t)} \left(\sum_{i(t)\in\mathbf{I}(t)} \gamma_{i,j}(t)\right)\right)^2}{J(t)\left(\sum_{j(t)\in\mathbf{J}(t)} \left(\sum_{i(t)\in\mathbf{I}(t)} \gamma_{i,j}(t)\right)^2\right)}, \tag{8c}$$

$$0 \leq \beta_{i,j}(t) \leq 1, \tag{8d}$$

To fulfill the data rate requirement of $Q_{i,j}(t)$, the number of resource blocks required is denoted by $r_{i,j}(t)$ in (8a). $\gamma_{i,j}(t)$ in (8b) is the normalized number of resource block by associated IoT devices with a LEO-cloudlet. $\beta_{i,j}(t)$ in (8c) is the RFI and it's value ranges between zero and one shown in (8d). The value of RFI is one when the allocation of resource blocks to IoT devices follow optimum fairness.

C. *Task offloading model*

In this cellular environment, there are two modes to fulfill the data storage, and computation requests by the $I(t)$ IoT devices,i.e., LEO-cloudlet mode or GEO-cloud mode. LEO-cloudlet mode is the first choice of the IoT device since involves little latency due to less distance between IoT device and LEO-cloudlet. Second choice is the GEO-cloud mode if the data storage, and computation request by the IoT device $i(t) \in \mathbf{I}(t)$ is not fulfilled by the LEO-cloudlet $j(t) \in \mathbf{J}(t)$. The detail of two modes is given below:

1) **LEO-cloudlet mode:** Let the IoT device $i(t) \in \mathbf{I}(t)$ is operating in the far flung area and records two data files $f^s_{i,j}(t)$ and $f^c_{i,j}(t)$ from the surrounding environment. The $f^s_{i,j}(t)$ and $f^c_{i,j}(t)$ are the data files to be stored, and computed, respectively, by the IoT device $i(t) \in \mathbf{I}(t)$ to the LEO-cloudlet $j(t) \in \mathbf{J}(t)$. The Ω^{LEO}_s and Ω^{LEO}_c are storage and computation capacity of the LEO-cloudlet, respectively. The storage and computation tasks need to be performed by LEO-cloudlet $j(t) \in \mathbf{J}(t)$. These tasks are scheduled, queued, and transmitted to be accomplished in available N time windows. Latency experienced while completing these tasks is given below:

$$l^{\text{LEO}}_{i,j,q}(t) = \tau(N-1), \tag{9a}$$

$$l^{\text{LEO}}_{i,j,m}(t) = \frac{f^{\text{s}}_{i,j}(t) + f^{\text{c}}_{i,j}(t)}{\psi_{i,j}(t)}, \tag{9b}$$

$$l^{\text{LEO}}_{i,j,\rho}(t) = \frac{s_{i,j}(t)}{\upsilon}, \tag{9c}$$

$$l^{\text{LEO}}_{i,j,c}(t) = \eta\left(\frac{f^{\text{c}}_{i,j}(t)}{\Omega^{\text{LEO}}_c}\right), \tag{9d}$$

$$l^{\text{LEO}}_{i,j,T}(t) = l^{\text{LEO}}_{i,j,q}(t) + l^{\text{LEO}}_{i,j,m}(t) + l^{\text{LEO}}_{i,j,\rho}(t) + l^{\text{LEO}}_{i,j,c}(t), \tag{9e}$$

where $l^{\text{LEO}}_{i,j,q}(t)$ is the queue delay, $l^{\text{LEO}}_{i,j,m}(t)$ is the transmission delay, $l^{\text{LEO}}_{i,j,\rho}(t)$ is the propagation delay, $l^{\text{LEO}}_{i,j,c}(t)$ is the computing delay, and $l^{\text{LEO}}_{i,j,T}(t)$ is the total delay occur while completing the tasks of the IoT device $i(t) \in \mathbf{I}(t)$. The η is the number of CPU cycles required to compute the data at LEO-cloudlet and Ω^{LEO}_c is computing ability of the LEO-cloudlet in cycles/second. The $s_{i,j}(t)$ is the distance between IoT device $i(t) \in \mathbf{I}(t)$ and LEO-cloudlet $j(t) \in \mathbf{J}(t)$. The τ is the length of a time window, N is the total time windows.

2) **GEO-cloudlet mode:** GEO-cloud is contacted if the request by IoT device $i(t) \in \mathbf{I}(t)$ to store and compute the data files is not entertained by the LEO-cloudlet $j(t) \in \mathbf{J}(t)$. LEO-cloudlet $j(t) \in \mathbf{J}(t)$ sends the request to store and compute the data files to GEO-cloud. As the distance involved between LEO-cloudlet and GEO-cloud is very much high, so propagation delay involved will add too much latency to fulfill the request of IoT device $i(t) \in \mathbf{I}(t)$. In this case, the propagation delay [38] involved in storing and computing the requested data files is given below:

$$l^{\text{GEO}}_{i,j,\rho}(t) = \frac{s^{\text{GEO}}_j(t)}{\upsilon}, \tag{10a}$$

$$l^{\text{GEO}}_{i,j,c}(t) = \eta\left(\frac{f^{\text{c}}_{i,j}(t)}{\Omega^{\text{GEO}}_c}\right), \tag{10b}$$

$$l^{\text{GEO}}_{i,j,T}(t) = l^{\text{GEO}}_{i,j,\rho}(t) + l^{\text{GEO}}_{i,j,c}(t). \tag{10c}$$

The propagation delay $l^{\text{GEO}}_{i,j,\rho}(t)$ is distance dependent where $s^{\text{GEO}}_j(t)$ is the distance between LEO-cloudlet $j(t) \in \mathbf{J}(t)$ and GEO-cloud, and Ω^{GEO}_c is computing ability of the GEO-cloud in cycles/second. Using Eq. (9) and (10), the maximum latency experienced in this communication environment is given below:

$$l_{i,j}(t) = z_{i,j}(t) l^{\text{LEO}}_{i,j,T}(t) + \left(1 - z_{i,j}(t)\right) l^{\text{GEO}}_{i,j,T}(t), \tag{11}$$

TABLE II
LIST OF ABBREVIATIONS AND NOTATIONS

Definitions	Abbreviations	Definitions	Notations
Geosynchronous Earth Orbit	GEO	Set of IoT devices	$\mathbf{I}$
Low Earth Orbit	LEO	Set of cloudlets	$\mathbf{J}$
Internet of Things	IoT	Set of data files stored	$\mathbf{S}$
Satellite Assisted Internet of Things	S-IoT	Set of data files computed	$\mathbf{C}$
Resource Blocks	RBs	Admission indicator	x_i
Quality of Services	QoS	Association indicator	$y_{i,j}$
Energy Efficiency	EE	IoT fairness index	$\alpha_{i,j}$
Mixed Integer Non-Linear programming	MINLP	Max power of IOT device	P_i
Non-Linear Programming	NLP	Power allocated by IoT device in the UL	$p_{i,j}$
Mixed Integer Linear Programming	MILP	Channel gain between IoT device and LEO-cloudlet	$h_{i,j}$
Non-deterministic polynomial-time hard	NP-Hard	Transmit Antenna gain of IoT device	G_i^{Tx}
Charnes Cooper Transformation	CCT	Receive Antenna gain of LEO-cloudlet	G_j^{Rx}
Concave Fractional Programming	CFP	Minimum QoS data rate	$\Psi_{i,j}$
Outer Approximation Algorithm	OAA	Maximum allowed QoS latency	$D_{i,j}$
Exhaustive Search Algorithm	ESA	Minimum QoS UFI	Q_{UFI}
Basic Open-source Nonlinear Mixed Integer Programming	BONMIN	Minimum QoS RFI	Q_{RFI}
Floating-point Operation	Flop	Attenuations in Channel	$\xi_{i,j}(t)$
Cycle Per Unit	CPU	Channel Bandwidth	$b_{i,j}(t)$
Task Nodes	TNs	Number of Resource Block	$\gamma_{i,j}(t)$
Upper Bound	UB	Signal to interference and Noise Ratio	$\Phi_{i,j}(t)$
Lower Bound	LB	Intensity of Rain Fall	$\Re^{\mu_r}$

where $l_{i,j}(t)$ is the maximum delay which can be caused to a IoT device while completing its tasks.

D. *Energy consumption model*

The transmission energy and circuit energy are the two categories which are considered in the optimization technique for energy consumption model in the UL. Circuit energy includes the circuit components, i.e., amplifiers, convertors, and processing units etc. The transmission energy is the transmitter energy used while sending the data in the UL. The circuit energy and the transmission energy are denoted by P_c and $p_{i,j}$, respectively [39]. Mathematically, the total energy consumed by the IoT device $i(t) \in \mathbf{I}(t)$ to send data to the LEO-cloudlet $j(t) \in \mathbf{J}(t)$ is given below:

$$P_{total} = P_c + p_{i,j}. \tag{12}$$

The EE is calculated as follows based on the proportion of transferred data to energy used:

$$EE = \frac{\psi_{i,j}}{P_{total}}, \tag{13}$$

where the units of $\psi_{i,j}(t)$ and P_{total} are bits per second and watts, respectively. Therefore, the unit of EE is bits/sec/watt.

E. *Problem formulation*

For the network depicted in Fig. 1, we now formulate the joint admission control, association of IoT devices, and allocation of power problem. Fairness in the assignment of $I(t)$ IoT nodes to $J(t)$ LEO-cloudlets is also a factor in this dilemma. Allocating chunks of spectrum to IoT devices in the network is done in a fair manner. To begin, we will define the objective function and the limitations.The ultimate segment of the paper entails the formulation of the mathematical model pertaining to the issue at hand. The goal function and its constraints are described below.

- **Objective function:** Using (2), (5), (7), (12), and (13), EE maximization/optimization is the objective of this research work and defined below:

$$EE = \frac{\sum\limits_{j(t)\in\mathbf{J}(t)} \sum\limits_{i(t)\in\mathbf{J}(t)} y_{i,j}(t)\psi_{i,j}(t)}{P_c + \sum\limits_{j(t)\in\mathbf{J}(t)} \sum\limits_{i(t)\in\mathbf{I}(t)} p_{i,j}}. \tag{14}$$

- **IoT device association:** Using (2), the constraints that ensures association of IoT device $i(t) \in \mathbf{I}(t)$ with just one LEO-cloudlet $j(t) \in \mathbf{J}(t)$ is given below:

$$\sum_{j(t)\in\mathbf{J}(t)} y_{i,j}(t) \leq 1 \; \forall \; i(t) \in \mathbf{I}(t). \tag{15}$$

- **Power allocation:** If the Internet-of-Things device $i(t) \in \mathbf{I}(t)$ is allowed into the network, it will receive the power allocation $p_{i,j}(t)$. The following constraint ensures that power is allocated to each admitted IoT device using (1) and (5).

$$0 \leq x_i(t)p_{i,j}(t) \leq P_i, \; \forall \; i(t) \in \mathbf{I}(t), \; j(t) \in \mathbf{J}(t), \tag{16}$$

- **Achieved data rate versus QoS data rate:** Another QoS requirement is the minimum data rate required to complete the offloading tasks if IoT device $i(t) \in \mathbf{I}$ is admitted in the network . In order to guarantee a certain level of quality of service, the minimum data rate required to do so is constrained by (1), (5), (6), and (7).

$$\psi_{i,j}(t) \geq x_i(t)\Psi_{i,j}, \ \forall\, i(t) \in \mathbf{I}(t), \ j(t) \in \mathbf{J}(t), \tag{17}$$

- **Achieved data rate versus QoS latency:** Another QoS requirement for the admitted IoT device is that achieved data rate should be such that maximum latency threshold is not compromised. The constraint to guarantee an adequate data rate for quality of service is stated here using (1), (5), (6), and (7).

$$\psi_{i,j}(t) \geq x_i(t)\left(\frac{f^{\mathrm{s}}_{i,j}(t) + f^{\mathrm{c}}_{i,j}(t)}{D_{i,j}(t)}\right), \ \forall\, i(t) \in \mathbf{I}(t), \ j(t) \in \mathbf{J}(t), \tag{18}$$

- **Latency:** One of the quality of service (QoS) requirement is the minimum latency in accomplishment of task offloading to the LEO-cloudlet. Using (3), (9), (10), and (11), the constraint to ensure QoS minimum latency is given below:

$$l_{i,j}(t) \leq x_i(t)L_{i,j}, \ \forall\, i(t) \in \mathbf{I}(t), \ j(t) \in \mathbf{J}(t), \tag{19}$$

- **LEO-cloudlet storage:** The constraints that ensures sum of data size of files to be store at LEO-cloudlet $j(t) \in \mathbf{J}(t)$ is with in its storage capacity is given below:

$$\sum_{i(t)\in\mathbf{I}(t)} z_{i,j}(t) f^{\mathrm{s}}_{i,j}(t) \leq \Omega^{\mathrm{LEO}}_{s} \ \forall\, i(t) \in \mathbf{I}(t). \tag{20}$$

- **Fairness in IoT device association:** The distribution of $I(t)$ IoT devices traffic load in terms of association with $J(t)$ LEO-cloudlets should follow fairness to avoid over loading of a LEO-cloudlet. Using (4), the constraint to ensure fairness in distribution IoT devices traffic is given below:

$$\alpha_{i,j}(t) \geq x_i Q_{\mathrm{UFI}}, \ \forall\, i(t) \in \mathbf{I}(t), \ j(t) \in \mathbf{J}(t). \tag{21}$$

- **Fairness in RBs allocation:** The distribution of $I(t)$ IoT devices traffic load should follow fairness to avoid overloading and underloading of $J(t)$ LEO-cloudlets. Using (8), the constraint to ensure fairness in distribution RBs is given below:

$$\beta_{i,j}(t) \geq x_i Q_{\mathrm{RFI}}, \ \forall\, i(t) \in \mathbf{I}(t), \ j(t) \in \mathbf{J}(t). \tag{22}$$

Objective function and constraints defined in (14) - (22) helps in formulating a mathematical model to achieve latency aware resource allocation, i.e., fairness in IoT device association and resource blocks allocation etc and task offloading in GEO-LEO Satellite Networks. Table II provides a concise overview of the annotations and representations commonly employed when posing a problem. To achieve throughput maximization in GEO-LEO satellite networks, the mathematically problem with objective function $\mathbb{U}$ is given below:

$$\max_{y,p} \ \frac{\sum_{j(t)\in\mathbf{J}(t)} \sum_{i(t)\in\mathbf{I}(t)} y_{i,j}(t)\psi_{i,j}(t)}{P_c + \sum_{j(t)\in\mathbf{J}(t)} \sum_{i(t)\in\mathbf{I}(t)} p_{i,j}} \tag{23a}$$

$$\text{s.t.} \sum_{j(t)\in\mathbf{J}(t)} y_{i,j}(t) \leq 1 \ \forall\, i(t) \in \mathbf{I}(t), \tag{23b}$$

$$0 \leq x_i(t)p_{i,j}(t) \leq P_i, \ \forall\, i(t) \in \mathbf{I}(t), \ j(t) \in \mathbf{J}(t), \tag{23c}$$

$$\psi_{i,j}(t) \geq x_i(t)\Psi_{i,j}, \ \forall\, i(t) \in \mathbf{I}(t), \ j(t) \in \mathbf{J}(t), \tag{23d}$$

$$\psi_{i,j}(t) \geq x_i(t)\left(\frac{f^{\mathrm{s}}_{i,j}(t) + f^{\mathrm{c}}_{i,j}(t)}{L_{i,j}(t)}\right), \forall\, i(t) \in \mathbf{I}(t), \ j(t) \in \mathbf{J}(t), \tag{23e}$$

$$l_{i,j}(t) \leq x_i(t)L_{i,j}, \ \forall\, i(t) \in \mathbf{I}(t), \ j(t) \in \mathbf{J}(t), \tag{23f}$$

$$\sum_{i(t)\in\mathbf{I}(t)} z_{i,j}(t) f^{\mathrm{s}}_{i,j}(t) \leq \Omega^{\mathrm{LEO}}_{s} \ \forall\, j(t) \in \mathbf{J}(t), \tag{23g}$$

$$\alpha_{i,j}(t) \geq x_i Q_{\mathrm{UFI}}, \ \forall\, i(t) \in \mathbf{I}(t), \ j(t) \in \mathbf{J}(t), \tag{23h}$$

$$\beta_{i,j}(t) \geq x_i Q_{\mathrm{RFI}}, \ \forall\, i(t) \in \mathbf{I}(t), \ j(t) \in \mathbf{J}(t). \tag{23i}$$

Each IoT device, denoted as $i(t) \in \mathbf{I}(t)$, is constrained to associate with only one LEO-cloud, represented as $j(t) \in \mathbf{J}(t)$, as stipulated by constraint (23b). The power allocation for an admitted IoT device, $i(t) \in \mathbf{I}(t)$, during uplink (UL) transmission must not exceed the available maximum power, ensuring compliance with constraint (23c). Constraint (23d) guarantees that the achieved data rate of an IoT device surpasses the minimum Quality of Service (QoS) data rate requirement. Similarly, constraint (23e) guarantees that the data transmission time for achieving the data rate of an IoT device remains within the specified QoS latency threshold. This latency constraint is bounded by the QoS maximum threshold, as stated in constraint (23f). Additionally, the cumulative size of data files designated for storage within a LEO-cloudlet must not exceed the storage capacity of the LEO-cloudlet, as ensured by constraint (23g). Constraint (23h) emphasizes fairness in the traffic offloading of IoT devices, while constraint (23i) guarantees equitable allocation of resource blocks among the IoT devices.

F. Alternate Technique

The problem expressed in (23) involves both numerator and denominator functions that are concave and convex. The real-valued functions $\psi_{i,j}(t)$ and $p_{i,j}(t)$ are defined within a subset of R^n, rendering it a classic instance of Concave Fractional Programming (CFP). To transform this CFP problem into a concave optimization problem, we employ the Charnes Cooper Transformation (CCT) technique [40]. By substituting $p_{i,j}(t) = \left(\frac{u_{i,j}(t)}{v}\right)$, the optimization problem can be reconfigured into an equivalent concave form. Following the required substitutions in (23), the transformed concave optimization problem is presented.

$$\max_{y,p} \quad v \sum_{j(t)\in\mathbf{J}(t)} \sum_{i(t)\in\mathbf{J}(t)} y_{i,j}(t) b_{i,j}(t) log_2 \left(1 + \frac{u_{i,j}(t) h_{i,j}(t)}{v\left(I_{i',j}(t) + \sigma^2\right)}\right), \tag{24a}$$

$$\text{s.t.} \sum_{y(t)\in\mathbb{Y}(t)} \beta_{x,y}(t) \leq 1 \; \forall \, x(t) \in \mathbb{X}(t), \tag{24b}$$

$$0 \leq x_i(t) u_{i,j}(t) \leq v P_i, \; \forall \, i(t) \in \mathbf{I}(t), \; j(t) \in \mathbf{J}(t), \tag{24c}$$

$$y_{i,j}(t) b_{i,j}(t) log_2 \left(1 + \frac{u_{i,j}(t) h_{i,j}(t)}{v\left(I_{i',j}(t) + \sigma^2\right)}\right) \geq x_i(t) \Psi_{i,j}, \quad \forall \, i(t) \in \mathbf{I}(t), \; j(t) \in \mathbf{J}(t), \tag{24d}$$

$$y_{i,j}(t) b_{i,j}(t) log_2 \left(1 + \frac{u_{i,j}(t) h_{i,j}(t)}{v\left(I_{i',j}(t) + \sigma^2\right)}\right) \geq x_i(t) \left(\frac{f^{\mathrm{s}}_{i,j}(t) + f^{\mathrm{c}}_{i,j}(t)}{L_{i,j}(t)}\right), \; \forall \, i(t) \in \mathbf{I}(t), \; j(t) \in \mathbf{J}(t), \tag{24e}$$

$$l_{i,j}(t) \leq x_i(t) L_{i,j}, \; \forall \, i(t) \in \mathbf{I}(t), \; j(t) \in \mathbf{J}(t), \tag{24f}$$

$$\sum_{i(t)\in\mathbf{I}(t)} z_{i,j}(t) f^{\mathrm{s}}_{i,j}(t) \leq \Omega^{\mathrm{LEO}}_s \; \forall \, j(t) \in \mathbf{J}(t), \tag{24g}$$

$$\alpha_{i,j}(t) \geq x_i Q_{\mathrm{UFI}}, \; \forall \, i(t) \in \mathbf{I}(t), \; j(t) \in \mathbf{J}(t), \tag{24h}$$

$$\beta_{i,j}(t) \geq x_i Q_{\mathrm{RFI}}, \; \forall \, i(t) \in \mathbf{I}(t), \; j(t) \in \mathbf{J}(t), \tag{24i}$$

$$P_c v + \sum_{j(t)\in\mathbf{J}(t)} \sum_{i(t)\in\mathbf{I}(t)} u_{i,j}(t) = 1. \tag{24j}$$

Therefore, the challenge outlined in (24) falls into the category of predicaments recognized as conventional Mixed-Integer Non-Linear Programming (MINLP) predicaments. The intricate task of associating IoT devices with LEO-cloudlets and determining their respective UL power allocations [41] constitutes a sophisticated and challenging NP-hard problem. The optimization problem presented in (24) possesses a combinatorial nature. To surmount this formidable challenge, one potential approach is to employ a brute-force algorithm. This approach involves an exhaustive search, systematically exploring and evaluating each option until the optimal solution is achieved. However, when aiming for the best possible solution, the algorithm would need to navigate a search space that grows exponentially with the number of connected devices, or $2^{|I|}$. Moreover, the complexity of the algorithm escalates as the count of simulated IoT devices increases. Alternatively, a more streamlined approach to attaining the $\epsilon = 10^{-3}$ optimal solution involves the use of outer approximation.

III. Proposed Algorithm - Outer Approximation

The challenge presented in (24) constitutes a MINLP problem involving a combination of linear, non-linear, and binary variables. The Outer Approximation Algorithm (OAA) dissects the MINLP problem outlined in (24) into two distinct sub-problems, enumerated as follows:

- Sub-problem NLP.
- Sub-problem MILP.

The complexity of the two sub-problems is manageable, and the OAA efficiently achieves an optimal solution within a specific number of iterations [42], [43].

A. Description of Outer Approximation Algorithm

Let us assume that both the objective function and the constraints of the problems presented in (24) are represented as Θ and $\Pi_{\text{24b-24j}}$, respectively. Binary variables are denoted by $\mathbf{T}$, where $\mathbf{T} = x_i, y_{i,j}$. Furthermore, we define $\mathbf{N} = u_{i,j}$ and $\mathbf{M} = \mathbf{T} \cup \mathbf{N}$. For the aforementioned problems in (24), the following four propositions hold true:

1) The set $\mathbf{N}$ is nonempty, convex, and compact.
2) Both Θ and $\Pi_{\text{24b-24j}}$ are convex with respect to $\mathbf{N}$ for a certain constant $\mathbf{M}$.
3) Differentiation can be performed on Θ and $\Pi_{\text{24b-24j}}$ for a specific $\mathbf{M}$.
4) To enable a precise solution for a MINLP problem, it is necessary to first establish a fixed $\mathbf{M}$.

*1) **Sub-problem NLP**:* In order to convert MINLP problems similar to those described in (24) into NLP problems, the value of $\mathbf{M}$ needs to be fixed at $\mathbf{M}^k$ during the initial stage. The upper bound (UB) of the optimal solution serves as the solution to the NLP problem. The formulation of the challenge can be stated as follows:

$$\min_{\mathbf{N}} \quad -\Theta(\mathbf{M}^k, \mathbf{N}) \tag{25a}$$

$$\text{s.t.} \quad \Pi_{\text{24b-24j}}(\mathbf{M}^k, \mathbf{N}) \leq 0 \tag{25b}$$

*2) **Sub-problem MILP**:* By employing the solution derived from the NLP problem presented in (25), we can acquire the binary variables of $\mathbf{M}$ at $\mathbf{M}^k$. The MINLP problems in (24) are then converted into an MILP problem utilizing the outcomes from the initial stage. The MILP problem can be succinctly described as follows:

$$\min_{\mathbf{M}} \min_{\mathbf{N}} \quad -\Theta(\mathbf{M}^k, \mathbf{N}) \tag{26a}$$

$$\text{s.t.} \quad \Pi_{\text{24b-24j}}(\mathbf{M}^k, \mathbf{N}) \leq 0 \tag{26b}$$

(26) can also be written as:

$$\min_{\mathbf{M}} \quad -\varpi(\mathbf{M}) \tag{27}$$

such that

$$\varpi(\mathbf{M}) \quad = \min_{\mathbf{N}} \; -\Theta(\mathbf{M}^k, \mathbf{N}) \tag{28a}$$

$$\text{s.t.} \quad \Pi_{\text{24b-24j}}(\mathbf{M}^k, \mathbf{N}) \leq 0 \tag{28b}$$

(24) projected onto $\mathbf{M}$-space presents the difficulty described in (27). For every $\mathbf{M}^k$, the constraints for the NLP issue stated in (25) hold, hence the projection problem may be expressed as follows:

$$\min_{\mathbf{M}} \min_{\mathbf{N}} \quad -\Theta(\mathbf{M}^k, \mathbf{N}^k) - \nabla\Theta(\mathbf{M}^k - \mathbf{N}^k) \begin{pmatrix} \mathbf{N} - \mathbf{N}^k \\ \mathbf{M} - \mathbf{M}^k \end{pmatrix} \tag{29a}$$

$$\text{s.t.} \quad \Pi_{\text{24b-24j}}(\mathbf{M}^k, \mathbf{N}^k) - \nabla\Pi_{\text{24b-24j}}(\mathbf{M}^k, \mathbf{N}^k) \begin{pmatrix} \mathbf{N} - \mathbf{N}^k \\ \mathbf{M} - \mathbf{M}^k \end{pmatrix} \leq 0. \tag{29b}$$

The issue in (29) can be rewritten as follows by substituting ς for another variable:

$$\min_{\mathbf{M},\mathbf{N},\varsigma} \quad \varsigma \tag{30a}$$

$$\text{s.t.} \quad \varsigma \geq -\Theta(\mathbf{M}^k,\mathbf{N}^k) - \nabla\Theta(\mathbf{M}^k-\mathbf{N}^k)\begin{pmatrix}\mathbf{N}-\mathbf{N}^k\\ \mathbf{M}-\mathbf{M}^k\end{pmatrix} \tag{30b}$$

$$\Pi_{24b\text{-}24j}(\mathbf{M}^k,\mathbf{N}^k) - \nabla\Pi_{24b\text{-}24j}(\mathbf{M}^k,\mathbf{N}^k)\begin{pmatrix}\mathbf{N}-\mathbf{N}^k\\ \mathbf{M}-\mathbf{M}^k\end{pmatrix} \leq 0 \tag{30c}$$

The MILP problem yields an optimal lower bound (LB) as shown in equation (30). To solve the MILP problem [44], the branch and bound approach is employed. Specifically, the MILP problem is motivated by the solution to the NLP problem at $\mathbf{M}^k$ [45], [46], assuming linearity of the objective function Θ and constraint function $\Pi_{24b\text{-}24j}$. The ϵ-optimal algorithm operates through the following iterative phases:

1) As the algorithm progresses towards an ϵ-optimal solution, the lower bound (LB) increases while the upper bound (UB) decreases.
2) When the difference between LB and UB becomes smaller than ϵ, the solution is deemed optimal.
3) If the difference exceeds ϵ, the binary variables $\mathbf{M}$ are updated to $\mathbf{M}^{k+1}$. Consequently, both the nonlinear programming (NLP) and mixed-integer linear programming (MILP) problems are resolved again in the subsequent iteration, yielding new LB and UB values.
4) The process of updating LB and UB continues until their difference becomes smaller than ϵ, indicating the achievement of the optimal solution.
5) The flowchart illustrating the ϵ-optimal algorithm is presented in Figure 2.

B. Algorithm Convergence and Optimality

The ϵ-optimal algorithm exhibits linear convergence, as indicated by [42], [45]. When the binary variables $\mathbf{M}$ are fixed at $\mathbf{M}^k$, the objective and constraint functions, namely Θ and $\Pi_{24b\text{-}24j}$, become convex. Utilizing the branch and cut technique, the ϵ-optimal algorithm [44] efficiently seeks the best solution (within $\epsilon = 10^{-3}$ iterations) when all four preconditions are fulfilled. This algorithm ensures that the obtained solution lies within an ϵ-bound of the optimal solution for any $\epsilon > 0$, a validity confirmed for smaller ϵ values. Regarding the provided binary variable $\mathbf{M}$, which dictates the optimality of $\mathbf{N}$ in accordance with (30), one potential solution is outlined below:

1) If $\varsigma \geq \Theta(\mathbf{M}^k,\mathbf{N}^k) \rightarrow$ *viable solution*
2) Otherwise $\varsigma \leq \Theta(\mathbf{M}^k,\mathbf{N}^k) \rightarrow$ *not a viable solution*

Hence, the MILP problem described in (30) does not possess an insolvable value of $\mathbf{M}^k$, ensuring that the ϵ-optimal algorithm converges within a finite number of iterations. As long as $\mathbf{M}$ remains constant, the algorithm consistently yields optimal outcomes due to the convex nature of both the objective and constraint functions. A comprehensive proof of convergence for the OAA algorithm is provided in [42]. Although an exhaustive search algorithm (ESA) could potentially find the optimal solution for problem in (24), it comes at the cost of exponentially increased processing time. The computational complexity of ESA can be expressed using the notation for complexity Ç and the I IoT devices:

$$\text{Ç}_{ESA} = 2^{2i} \tag{31}$$

On the other hand, OAA with an infinite number of iterations [43] will eventually lead you to the ϵ-optimal algorithm.

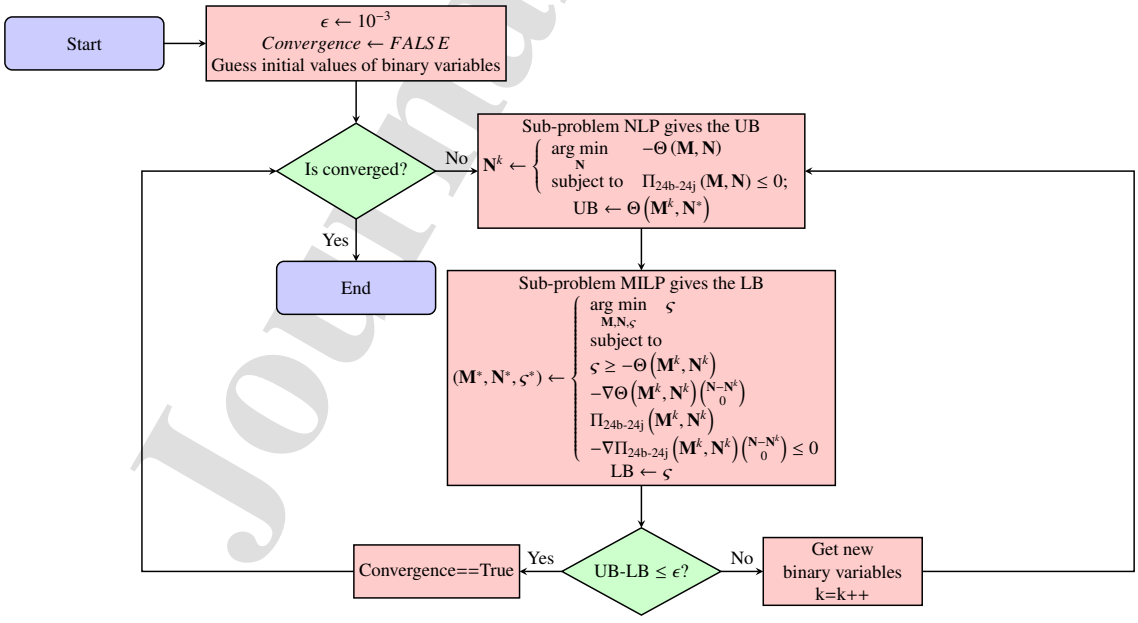

Fig. 2. **Flow chart - outer approximation algorithm**

Below is a simplified representation of the computational complexity of the OAA:

$$\zeta_{OAA} = \frac{i^2 \kappa}{\omega} \tag{32}$$

In the context provided, the variable κ signifies the total number of constraints, while ω represents the maximum permissible deviation of the ϵ-optimal method from the value of the global optimum. With OAA, you can be confident of attaining an optimal solution within the scope of ϵ, unlike ESA, where this assurance is lacking. The escalating computational complexity of both OAA and ESA is depicted in the referenced figure 3.

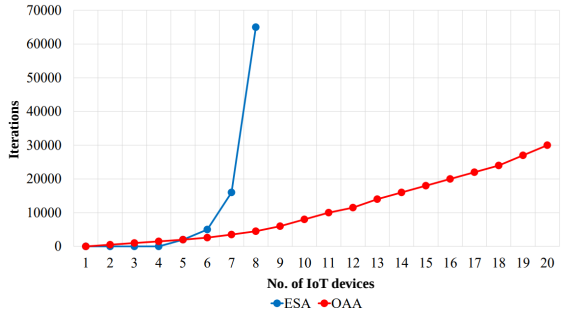

Fig. 3. **Number of IoT devices vs Computational Complexity - OAA and ESA.**

C. *Computational Complexity Analysis of the ϵ-Optimal Algorithm*

Assessing complexity sometimes involves the utilization of flops[1] [47]. In the initial stage of the epsilon-optimal algorithm, you will require five flops. To solve the NLP problem, simply include $4IJ\Upsilon$ and $2IJ$ flops. Solving the MILP problem demands an additional $2IJ\Upsilon$ and $4IJ\Upsilon$ flops. When considering both the NLP and MILP problems together, the algorithm accumulates a total of two flops. Incorporating additional binary values results in an additional four flops. The complexity of the ϵ-optimal algorithm can be assessed based on the number of flops essential for its completion.

$$E = 5 + 2IJ + 4IJ\Upsilon + 4IJ\Upsilon + 2IJ\Upsilon + 4, \tag{33a}$$

$$E = 9 + 2IJ + 10IJ\Upsilon, \tag{33b}$$

$$E \approx 2IJ + 10IJ\Upsilon. \tag{33c}$$

The complexity of the ϵ-optimal algorithm can be represented using Big O notation as $O(I\times J)+O(I\times J\times\Upsilon)$. Here, I denotes the number of connected IoT devices, J indicates the number of LEO cloudlets, and Υ represents the number of constraints in the problem.

[1]Counting the number of floating-point operations, or "flops," serves as a measure of complexity. Additionally, a flop is added each time a division or multiplication operation occurs. When combining two flops, complex addition is employed, while combining four flops employs complex multiplication. Performing matrix multiplication between a matrix of dimensions $l \times m$ and another matrix of dimensions $m\times o$ yields $2lmo$ flops. Both the logical operator and the assignment operator contribute one additional flop each. The operation $log_2(x)$ requires two flip-flops to complete

D. *Simulation Setup*

The simulations involved the utilization of various system parameters, as detailed in Table III. Throughout the simulation process, the maximum power for both Low Earth Orbit (LEO) and Geostationary Orbit (GEO) Satellites was established at 33 dBm and 37 dBm, respectively. The maximum radius was set to 1000 km for LEOs and 42000 km for GEO satellites. The minimum required data rates spanned from 0.2 Mbps to 1.0 Mbps. The minimum allowable number of users was set to 3, while the maximum allowable number was incrementally set to 48 in steps of 5. A total of 160 Resource Blocks (RBs) were available for user allocation. Other factors included a zero-mean Gaussian random variable set at 10 dB. The total circuit power (Pc) was defined as 10^{-6} Watts, and the maximum permissible latency was restricted to 5 ms. These parameters played a crucial role in conducting the simulations and assessing the system's performance.

TABLE III
SIMULATION PARAMETERS

Parameter	Value	Parameter	Value
P_l	33 dBm	R_j^{d}	{0.2,0.4,0.6,1.0} Mbps
P_g	37 dBm	R_j^{u}	{0.2,0.4,0.6,1.0} Mbps
HL	1,000 Km	HG	37,786 Km
T_{RB}	160‘	G	50
$b_{i,j}$	0.1 Mbps	$\xi_{i,j}(t)$	10 dB
P_c	-30 dBm	$l_{x,y}(t)$	5 ms
f_{l}^c	10^9 cycle/s	f_{g}^c	5×10^9 cycle/s
f_{l}^s	2 Gbps	f_{g}^s	50 Gbps
Min IOTs	3	Increment	5
Max IOTs	50	-	-

IV. RESULTS WITH IN-DEPTH DISCUSSIONS

In this section, the simulation outcomes are showcased, illustrating the efficacy of the proposed algorithm in accomplishing equitable admission control, IoT association, power allocation, and the maximization of EE. Furthermore, a performance evaluation is undertaken to discern the distinctions between the fairness-oriented approach and an approach devoid of fairness considerations. This assessment centers on IoT association, EE, and throughput within a hybrid satellite network encompassing GEO and LEO components.

Figure 4 depicts a graph showcasing the correlation between the quantity of IoT devices and IoT association (IoTA) (both fairness-based and without fairness). IoTA pertains to the cumulative count of accessible IoT devices as opposed to the count of IoT devices affiliated with the satellite network, encompassing both LEO and GEO satellites. The graph distinctly demonstrates that as the count of IoT devices escalates, there is a corresponding rise in IoTA, both under the fairness-based and non-fairness-based contexts. This indicates that with an augmentation in the network's device count, a higher likelihood exists for their connection with any available LEO/GEO satellite network.

The graph further reveals that the values of fairness-based and non-fairness-based IoTA are remarkably close, exhibiting

only a minor disparity in the overall mean count of affiliated devices. The noteworthy divergence lies in the just distribution of connected devices among the existing satellites in both scenarios. In the fairness-based IoTA approach, the association of devices with a particular LEO satellite takes into consideration the equitable distribution of load across the accessible satellite network. Conversely, in the absence of fairness-based IoTA, the device-to-satellite association does not consider the principle of equitably distributing the load.

Additionally, the graph in Figure 4 portrays a variety of satellites, encompassing both LEOs and GEOs, each characterized by distinct orbital velocities and QoS rates spanning from 0.2 to 1 Mbps. The findings conspicuously unveil that the count of IoT devices linked with GEO satellites notably trails behind other LEO satellites. This discrepancy can be attributed to several factors, including the extended propagation, processing, and transmission delays inherent in communicating with GEO satellites. Furthermore, the phenomenon of task offloading might transpire when LEO satellites are incapable of accommodating specific requests, leading to the redirection of these requests toward GEO satellites. As a result, GEO satellites manifest fewer affiliations with IoT devices compared to their LEO counterparts.

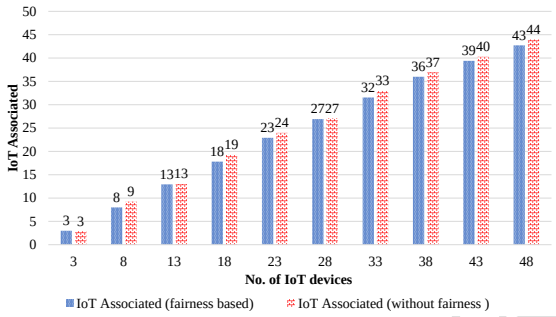

Fig. 4. **IoT devices vs IoT Devices Associated in hybrid GEO/LEO Satellite Network.**

Figure 5 provides a comparison between the findings from prior research [31] and [32], denoting the former as the baseline or previous condition, while the proposed curve with additional parameters portrays an upgraded or optimized scenario. The enhanced curve conspicuously illustrates a more streamlined and proficient resource allocation, leading to an increased count of IoT devices becoming part of the network. This progress signifies that the system has been refined to effectively manage the growing influx of IoT devices and cater to their connectivity demands. Moreover, the improved curve signifies that the system has implemented enhanced strategies for associating IoT devices, potentially involving optimized algorithms or resource allocation techniques. These advancements have contributed to a more judicious utilization of available resources, enabling a larger number of IoT devices to be successfully integrated into the network.

Figure 6 displays a graph illustrating the fairness-based IoTA in relation to different Quality of Service (QoS) rate requirements, spanning from 0.2 to 1.0 Mbps, for a total of 50 users. The primary focus of this plot is to showcase the

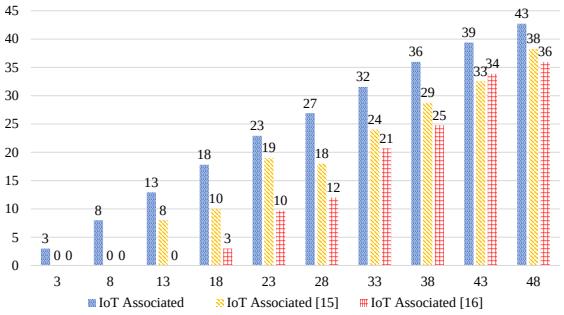

Fig. 5. **IoT devices vs IoT Devices Associated in comparison to paper 15 and 16.**

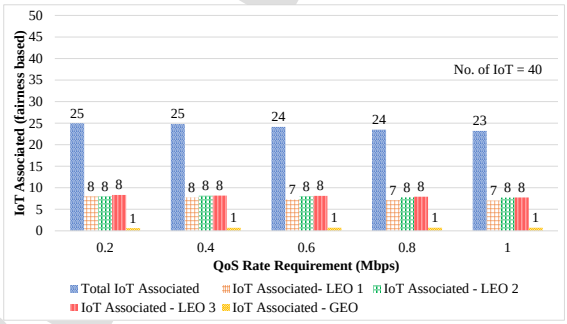

Fig. 6. **QoS Rate Requirement vs IoT Devices Associated (fairness based).**

distribution of device associations across both LEOs and GEO satellite networks. Upon a careful examination of Figure 6, it becomes evident that when the QoS rate requirement is set at 0.2 Mbps, there is an even distribution of devices among the available LEO satellites. Each LEO satellite accommodates a comparable number of associated devices, reflecting an equitable allocation of devices within the LEO satellite network. As the QoS rate requirement incrementally increases from 0.2 to 1.0 Mbps, the plot maintains a consistent trend similar to that observed at the 0.2 Mbps data rate.

Furthermore, the plot highlights that the number of devices connected to GEO satellites is notably lower compared to those associated with LEOs. This phenomenon stems from the primary role of LEO satellites in handling the generated requests from IoT devices, meeting the majority of their demands. Only a small fraction of requests that cannot be addressed by LEO satellites are redirected to GEO satellites. This allocation pattern is influenced by factors such as prolonged delays and response times linked with GEO satellites. Overall, the prominent presence of IoTA is witnessed with LEO satellites, irrespective of the data rate requirement, underscoring their pivotal role in facilitating connections for IoT devices. This pattern persists across both lower and higher data rates. Additionally, Figure 6 portrays a marginal decrease in the total count of associated devices as the Quality of Service (QoS) rate requirement progressively rises from 0.2 to 1.0 Mbps. This reduction in IoTA performance signifies that the system associates fewer devices as data rates increase, in comparison to instances with lower data rates.

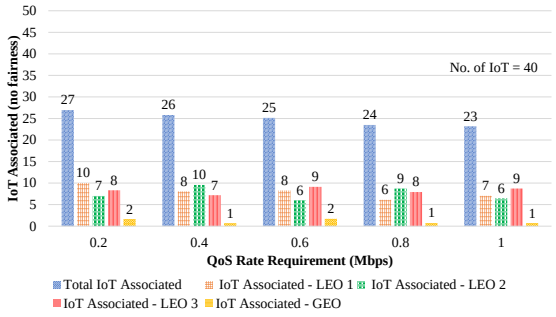

Fig. 7. **QoS Rate Requirement vs IoT Devices Associated (Without fairness).**

In figure 7, Uneven distribution of devices can result in congestion in certain areas or on specific satellite beams, leading to performance degradation and potential service disruptions. Unfair distribution of IoT devices may result in some devices receiving a disproportionately higher share of network resources, such as bandwidth or processing capabilities. This can lead to congestion, increased latency, and degraded performance for devices that receive inadequate resources. Consequently, the overall network efficiency and user experience may suffer.

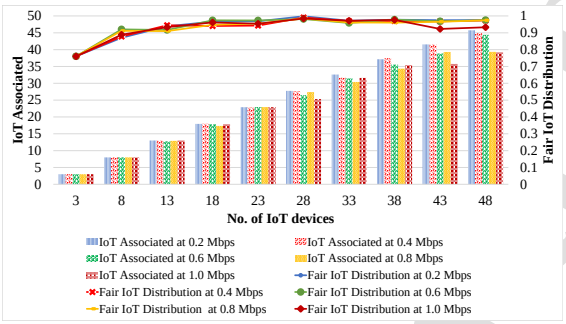

Fig. 8. **IoT Devices Associated vs IoT Devices at different QoS rate requirements**

Figure 8 provides a comprehensive plot that illustrates the interplay between the number of IoT devices, IoT Association (IoTA), and IoT Fairness (IoTF) index under varying Quality of Service (QoS) rate requirements—specifically, 0.2 Mbps, 0.4 Mbps, 0.6 Mbps, 0.8 Mbps, and 1.0 Mbps. The range of IoT devices spans from 3 to 50, with incremental steps of 5, facilitating a thorough analysis of the system's behavior across diverse IoT device quantities.

Of noteworthy significance is that even as IoTA diminishes in response to heightened QoS rate requirements, the fairness observed in associating devices with available LEOs and GEO satellites remains relatively stable across all examined QoS rate prerequisites—ranging from 0.2 Mbps to 1.0 Mbps. This discovery underscores the system's ability to uphold an equitable distribution of associations among the accessible satellite resources, regardless of the specific QoS rate demand. These findings serve as corroborative evidence to the outcomes presented in Figure 6 and 7, further affirming the consistency and resilience of our research findings.

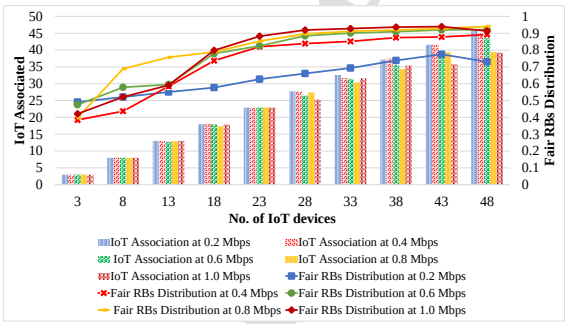

Fig. 9. **IoT Devices vs IoT Devices Associated and RB at different QoS rate requirements.**

Figure 9 provides a comprehensive analysis of how different Quality of Service (QoS) rate requirements influence the association of devices with Resource Blocks (RBs). The QoS rate requirement signifies the minimal acceptable data rate for each IoT device, exerting a significant influence on RB allocation. The graph's insights reveal that as the QoS rate requirement escalates, there is a slight reduction in the number of devices associated with RBs. This observation implies that higher data rate demands introduce limitations on resource availability, leading to a slightly lower count of devices being linked with RBs.

Notwithstanding the variations in device-RB associations across diverse QoS rate requirements, the graph highlights the system's adeptness in upholding a just distribution of RBs among IoT devices. This equity-based distribution guarantees that every device receives an equitable share of RBs according to its needs and the accessible resources. The observation underscores the system's efficacy in effectively managing resource allocation to maintain fairness, regardless of the specific QoS rate requirement. This aspect exemplifies the system's ability to optimally balance network performance with the individual requirements of IoT devices, ensuring equitable access to resources while catering to varying data rate demands.

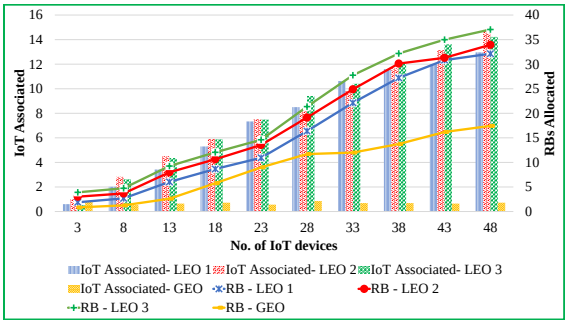

Fig. 10. **IoT Devices vs IoT Devices Associated and Allocated RBs.**

The graph 10 illustrates the allocation of RBs to the associated IoT devices. RB allocation represents the distribution of available RBs among the devices. It is evident from the graph

that as the number of IoT devices increases, the allocation of RBs also increases. This observation demonstrates that the system effectively manages RB allocation to accommodate the growing demand and ensure adequate resource provisioning for the associated devices.

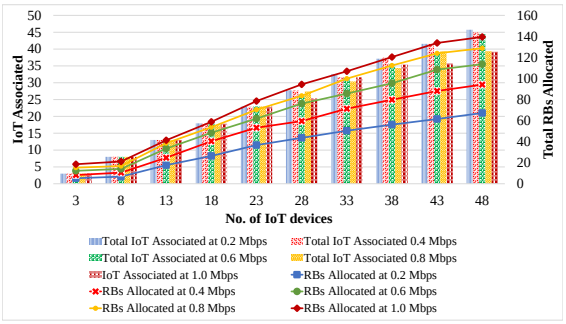

Fig. 11. **IoT Devices vs IoT Devices Associated and RB Fairness at different QoS rate requirements.**

Figure 11 provides an in-depth analysis of how distinct Quality of Service (QoS) rate requirements impact the association of devices with Resource Blocks (RBs). The QoS rate requirement denotes the minimum acceptable data rate for each IoT device, which significantly shapes RB allocation. The graph's insights reveal that as the QoS rate requirement rises, there is a marginal reduction in the number of devices affiliated with RBs. This observation implies that heightened data rate demands introduce limitations on resource availability, leading to a slightly diminished count of devices being linked with RBs.

Despite the variations in device-RB associations across diverse QoS rate requirements, the graph underscores the system's prowess in upholding equitable distribution of RBs among IoT devices. This fairness-driven distribution ensures that every device garners a proportionate allocation of RBs in line with its needs and the available resources. This observation reaffirms the system's adeptness in resource allocation management to ensure fairness, regardless of the specific QoS rate requirement. Such a capability showcases the system's effectiveness in optimizing network performance while accommodating individual IoT device requirements, ensuring just access to resources amidst varying data rate demands.

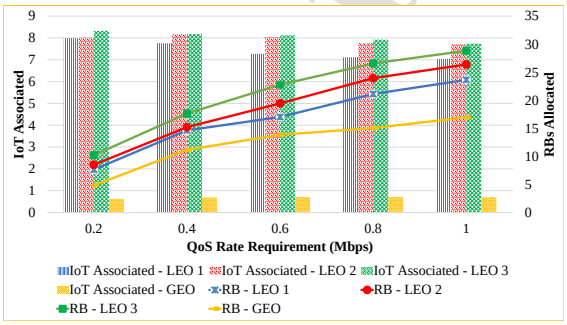

Fig. 12. **QoS rate requirement vs IoT Devices Associated and Allocated RBs.**

Figure 12 presents a graphical representation that elucidates the interplay between the Quality of Service (QoS) rate requirement of IoT devices and two key metrics: IoT association and Resource Block (RB) allocation. The graph unveils an inverse correlation between IoT association and the QoS rate requirement, while RB allocation exhibits a direct relationship with elevated QoS rate requirements. The graphical depiction in Figure 12 distinctly showcases that with the upsurge in the QoS rate requirement of IoT devices, the corresponding IoT association diminishes. This pattern aligns with expectations, given that higher data rates necessitate increased power consumption to uphold satisfactory performance levels. Consequently, at elevated data rates, the power needed for a user to affiliate with a specific LEO/GEO satellite network also rises. Consequently, the IoT association dwindles as the QoS rate requirement climbs.

Conversely, the RB allocation depicts a positive trajectory as the QoS rate requirement escalates. This signifies that augmented data rates call for a more extensive allotment of RBs or spectrum resources to cater to the heightened transmission demands. Hence, the allocation of RBs at elevated data rates surpasses that at lower data rates. This graph thus provides valuable insights into the intricate dynamics between QoS rate demands, IoT association, and RB allocation, underscoring the intricate balance required in optimizing network performance.

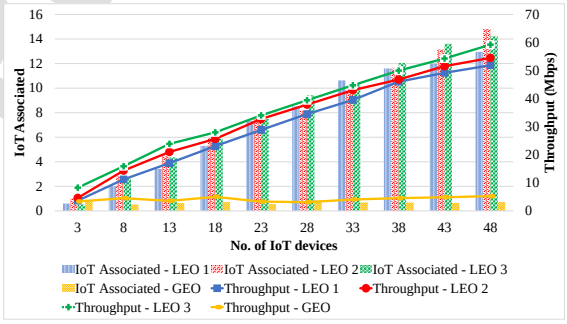

Fig. 13. **IoT Devices vs IoT Devices Associated and Throughput.**

The graph 13 showcases the relationship between the number of devices associated with the network and the resulting throughput. Throughput represents the rate at which data is transmitted through the network and is a crucial performance metric for IoT applications. The graph illustrates that as the number of associated devices increases, the throughput also tends to increase. This observation suggests that the network can efficiently handle the data transmission demands of a larger device population, leading to higher overall throughput. As the number of IoT devices grows, the network demonstrates its ability to scale and maintain higher throughput levels. This scalability is essential for ensuring that the network can handle the increasing data traffic and meet the performance requirements of IoT applications. By efficiently managing resources such as bandwidth, transmission power, and scheduling, the network can ensure that data is transmitted more effectively, thereby increasing throughput. This optimization takes into account factors like channel conditions, traffic patterns, and QoS requirements.

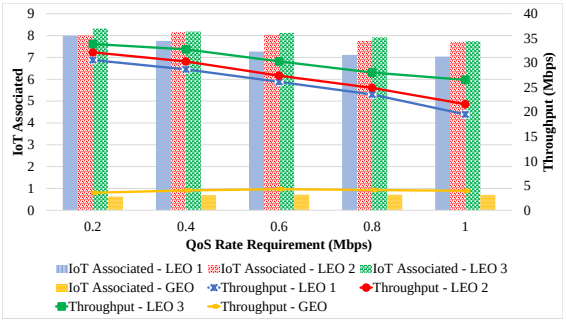

Fig. 14. **QoS rate requirement vs IoT Devices Associated and Throughput.**

In our analysis, we have delved into the impact of Quality of Service (QoS) rate requirements, which define the minimum acceptable data rate for each IoT device. Figure 14 portrays a graphical representation that elucidates the intricate relationship between the number of IoT devices, IoT association (IoTA), and throughput across different QoS rate requirements: 0.2 Mbps, 0.4 Mbps, 0.6 Mbps, 0.8 Mbps, and 1.0 Mbps.

The behavior observed in the IoTA metric resonates with our earlier discussed findings. The consistent pattern of increasing user count across all QoS rate requirements underscores the proportional rise in the number of IoT associations with the augmentation of devices. This phenomenon holds true, regardless of the specific QoS rate requirement.

Additionally, Figure 14 brings into focus the varying trends in throughput across distinct QoS rate requirements. Notably, optimal throughput is attained when the QoS rate requirement is at its minimum. However, as the QoS rate requirement escalates, a subsequent decrease in throughput is observed. It's important to emphasize that despite this decline, the overall trajectory of throughput exhibits an upward tendency in correspondence with the growing number of IoT devices. This insight showcases the intricate balance between QoS demands and network performance, affirming the complex dynamics at play in IoT ecosystem management.

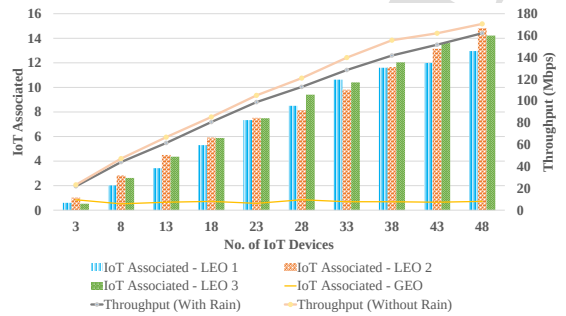

Fig. 15. **Throughput (With and Without Rain).**

Figure 15 depicts the behavior of throughput in the presence and absence of rain, as described by equation 6c. The curve clearly illustrates how throughput is influenced by the presence of rainy conditions when IoT devices are connected to LEO/GEO Satellites. It is evident that throughput decreases when rain is present, whereas it increases under clear weather conditions. The impact of rain on throughput is particularly noticeable when multiple devices are attempting to fetch their required data from the network. In cases where fewer devices are connected to the network, the effect of rain may not be as pronounced.

Under clear weather conditions, IoT devices can transmit data with higher signal strength and experience lower latency, resulting in smoother communication with the satellite network. The absence of rain reduces the likelihood of signal attenuation or signal loss, leading to improved overall connectivity. Raindrops falling through the signal path can cause signal absorption, scattering, and reflection, contributing to signal degradation. This attenuation in the signal strength can lead to increased noise and a higher bit error rate (BER), ultimately affecting the quality and reliability of the connection.

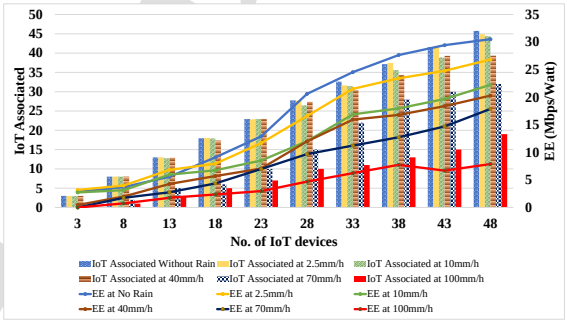

Fig. 16. **IoT Devices vs IoT Devices Associated and Energy Efficiency (without rain and different intensities of rain.**

Graph 16, depicting the correlation between rain intensity and energy efficiency in IoT devices, reveals a consistent pattern: with increasing rain intensities, both energy efficiency and IoT association exhibit a decline. This trend is particularly noticeable at exceptionally high levels of rain intensity, such as 100 mm/hr. Rainfall introduces signal attenuation, scattering, and interference, thereby degrading the quality and reliability of the wireless channel. As rain intensity escalates, these detrimental effects intensify, resulting in reduced energy efficiency due to the heightened energy requirements necessary to overcome the challenges posed by the compromised communication environment.

Furthermore, the reduction in IoT association can be attributed to the influence of rain intensities on connectivity. As rainfall becomes more intense, it obstructs data transmission, leading to increased packet loss and disruptions in communication. Consequently, IoT devices encounter difficulties in establishing and maintaining stable connections, ultimately resulting in a decrease in the number of successful IoT associations.

Graph 17 portrays the correlation between latency in IoT devices and their energy efficiency, thereby revealing a distinct pattern: an increment in latency is accompanied by a reduction in both energy efficiency and IoT association. The rise in latency signifies a prolonged delay in the transmission and reception of data between IoT devices and the network. This delay prompts heightened energy consumption, as devices

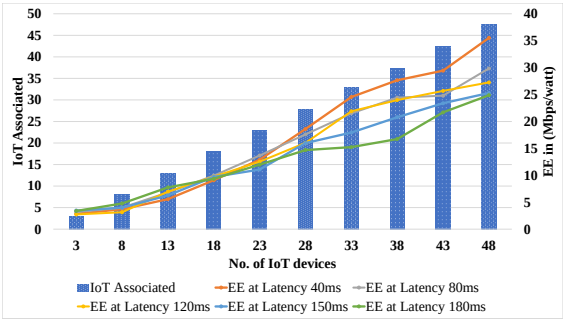

Fig. 17. **IoT Devices vs IoT Devices Associated and Energy Efficiency (at different latencies).**

must remain active for extended periods, awaiting responses or acknowledgments. Consequently, the energy efficiency diminishes, as more energy is expended per unit of transmitted data.

Furthermore, heightened latency exerts an adverse influence on IoT association. The delays in information exchange translate to postponed processing of commands and receipt of feedback. This delay-induced effect can lead to a curtailed number of successful associations between IoT devices, hampering their seamless connectivity and interaction with the network.

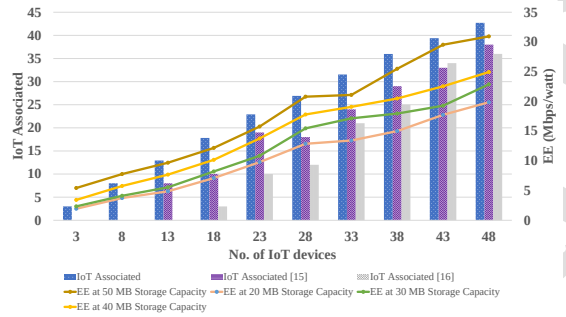

Fig. 18. **IoT Devices vs IoT Devices Associated and Energy Efficiency (at different Storage values).**

The graph 18 shows the relationship between IoT device storage values and energy efficiency uncovers a compelling trend: as storage increases, so does energy efficiency, accompanied by a boost in IoT association. Devices with more storage capacity can locally store and process more data. It reduces data transmission frequency to and from the network, resulting in reduced energy consumption. It can efficiently store and retrieve data as needed, reducing the need for frequent communication and increasing energy efficiency. Moreover, the increase in storage capacity positively impacts IoT association that allows devices to store more data locally, enabling them to operate autonomously and maintain continuous functionality even when network connectivity is intermittent or temporarily unavailable. It increases the likelihood of successful IoT associations as devices can maintain operations and synchronize data when network connectivity is restored.

Graph 19 portrays the interrelationship between the quantity of IoT devices and two crucial factors: the count of associated

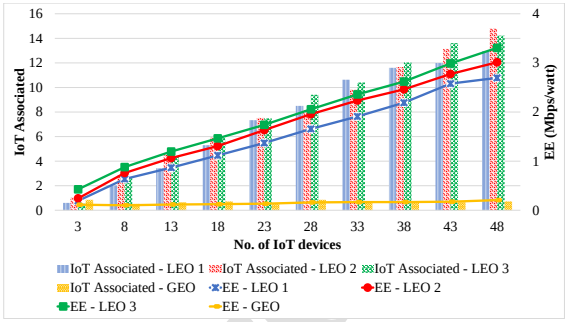

Fig. 19. **IoT Devices vs and IoT Associated and Energy Efficiency.**

IoT devices and their corresponding energy efficiency. The horizontal axis signifies the number of devices, spanning from 3 to 50, while the vertical axis represents the number of associated devices and their respective energy efficiency levels. The graph prominently indicates that with an escalating count of devices, the energy efficiency of the network experiences a gradual enhancement. This positive trend can be attributed to the amalgamation and optimization of resources across a larger device pool.

The upward trajectory in energy efficiency is a consequence of streamlined resource allocation and utilization strategies. As the number of devices increases, there emerges an amplified opportunity to streamline data processing and storage activities, thereby curtailing redundant energy consumption. This refined resource utilization fosters an improved energy efficiency landscape throughout the network.

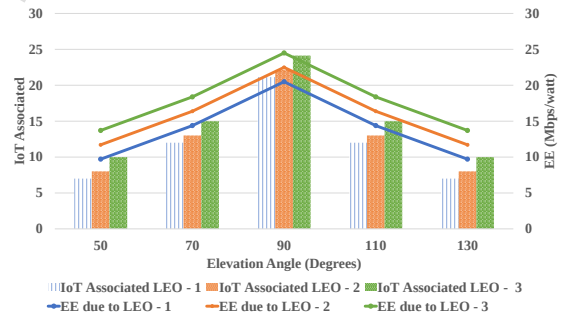

Fig. 20. **Angle of Elevation(degrees) vs IoT Devices Associated and Energy Efficiency.**

Graph 20 illustrates the correlation between the movement of a LEO satellite, its corresponding energy efficiency, and IoT association. The graph reveals that the maximum energy efficiency is achieved when an IoT device is positioned at a 90-degree angle to the LEO satellite. LEO satellites are characterized by their lower orbits around Earth, leading to shorter communication links and reduced signal propagation delays. When the IoT device is situated at a 90-degree angle, it aligns perfectly with the line of sight to the LEO satellite. This alignment enables direct and unobstructed communication between the device and the satellite.

In this optimal alignment, the IoT device receives the strongest and most reliable signals from the LEO satellite.

This efficient signal reception and transmission contribute to higher energy efficiency. Additionally, the ideal alignment enhances IoT association, as the device can establish a stable connection with the LEO satellite. This facilitates smooth data exchange and communication between the device and the satellite. However, as the angle deviates from 90 degrees, the alignment between the IoT device and the LEO satellite becomes less optimal. This can lead to decreased energy efficiency and potentially reduced IoT association due to signal degradation and increased signal propagation delays.

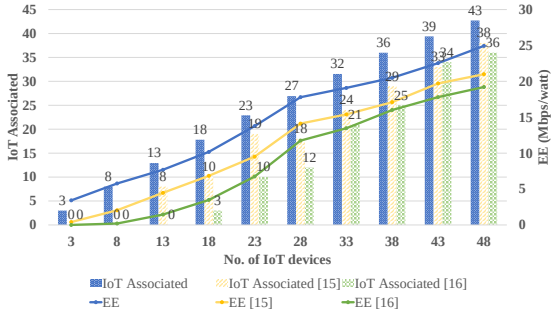

Fig. 21. **IoT Devices vs and IoT Associated and Energy Efficiency in comparison to paper 15 and 16.**

Graph 21 provides a comparison between the number of associated IoT devices and Energy Efficiency (EE) based on the approaches described in [31] and [32]. The curve labeled as [31] and [32] represents a previous scenario without IoT admission, processing, queuing delay factors, fair IoT distribution, and RB allocation. In this scenario, no considerations were made for optimizing energy efficiency. In contrast, the improved curve demonstrates a significantly higher level of energy efficiency compared to the previous scenario. This enhancement indicates that the system has implemented strategies to optimize energy usage and enhance the overall energy efficiency of the network. The improved curve suggests the utilization of energy-efficient algorithms, power management techniques, or resource allocation strategies to ensure the optimal use of energy resources. These improvements have led to a more efficient allocation of energy among the associated IoT devices, resulting in enhanced energy efficiency.

Moreover, the improved curve indicates that the system has achieved a better balance between IoT device association and energy efficiency. It shows that a greater number of IoT devices can be successfully associated with the network while maintaining or even improving energy efficiency. This signifies the successful integration of energy-efficient practices into the network design, ultimately benefiting both device connectivity and energy consumption.

Upon analyzing the graph depicted in Figure 22, noticeable trends and patterns emerge as the number of IoT devices increases, affecting both Energy Efficiency (EE) and Resource Blocks (RB) Allocation. Firstly, focusing on Energy Efficiency, it becomes apparent that EE tends to experience a gradual increase as the number of IoT devices rises. This observation suggests that, on average, the network becomes more energy-efficient when accommodating a larger number of IoT devices.

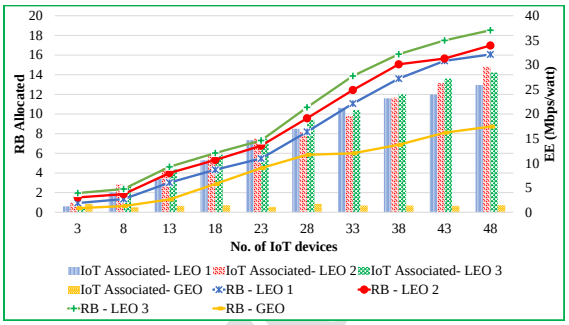

Fig. 22. **IoT Devices vs EE and RB Allocation.**

This positive correlation between device count and energy efficiency signifies improved resource utilization and optimized transmission strategies.

Conversely, RB Allocation pertains to the distribution of available resource blocks, fundamental units of wireless communication, among IoT devices. The graph underscores a similarity in the pattern between Energy Efficiency and RB Allocation. As the number of IoT devices increases, there is a corresponding rise in the allocation of resource blocks. This trend implies that the network adeptly manages its resources to cater to the demands of the expanding device population. A greater allocation of resource blocks facilitates enhanced connectivity, improved data transmission rates, and overall network performance.

Furthermore, the graph provides insights into the interplay between different allocation strategies and their impact on energy efficiency, as well as vice versa. This understanding can serve as a guide for the development of resource allocation algorithms and protocols that optimize both Energy Efficiency and RB Allocation. Such optimization efforts can lead to improved network performance, better sustainability, and more efficient resource utilization.

A. S-IoT network - case studies

Satellite-assisted IoT networks have emerged as a promising solution for achieving global connectivity, but they encounter challenges in effectively allocating resources due to the unique characteristics of satellite communication systems. This work introduces a solution to these challenges. The benefits of the proposed techniques are exemplified through various case studies:

- **Precision Agriculture Monitoring:** In remote agricultural areas, where terrestrial infrastructure is limited, satellite-assisted IoT networks play a crucial role in monitoring soil moisture, temperature, and crop health in real-time. By satellite-assisted IoT networks, farmers can optimize resource allocation for efficient data transmission, enabling timely insights into irrigation needs, pest infestations, and crop growth patterns. This not only enhances agricultural productivity but also conserves energy by ensuring that only essential data is transmitted.
- **Maritime Fleet Management:** Satellite-assisted IoT networks revolutionize maritime fleet management by en-

abling continuous monitoring of vessel location, engine performance, and cargo conditions. By satellite-assisted IoT networks, fleet operators can dynamically allocate bandwidth based on vessel priority, route optimization, and environmental conditions. This optimized resource allocation ensures seamless connectivity and efficient data transmission, leading to improved fleet safety, operational efficiency, and reduced fuel consumption.

- **Disaster Response and Emergency Management:** During natural disasters or humanitarian crises, rapid and reliable communication is essential for coordinating rescue efforts and delivering aid to affected areas. Satellite-assisted IoT networks provide resilient connectivity in disaster-stricken regions. This facilitates efficient disaster response and recovery operations, ultimately saving lives and minimizing damage.
- **Remote Environmental Monitoring:** In remote or environmentally sensitive areas such as wildlife reserves or ecological research sites, continuous environmental monitoring is crucial for conservation efforts and ecological research. Satellite-assisted IoT networks enable real-time data collection on biodiversity, habitat changes, and climate patterns. This data facilitates better conservation management, early detection of ecological threats, and informed decision-making for sustainable development initiatives.

These case studies illustrate how satellite-assisted IoT networks enriches the energy efficiency, and ensuring seamless connectivity across diverse applications and domains.

V. Conclusion

In summary, this study delves into the intricate domain of joint admission control, IoT association, and power allocation within the context of hybrid satellite-assisted Internet of Things (S-IoT) networks. The primary aim is to strike a balance between ensuring equitable IoT device association and spectrum resource allocation while optimizing energy efficiency (EE). Addressing this challenge involves tackling a Convex Fractional Programming (CFP) problem, which undergoes transformation into a concave optimization problem through the ingenious application of the Charnes-Cooper Transformation (CCT). The proposed Outer Approximation Algorithm (OAA) then comes to the forefront, tasked with resolving the concave optimization problem and deriving an epsilon ϵ optimum solution, with ϵ being set at 10^{-3}. The prowess of this ϵ-optimum solution, as orchestrated by the OAA, is scrutinized through the lens of diverse system parameters. These parameters encompass IoT association (IoTA), IoT fairness (IoTF), resource block (RB) fairness, and energy efficiency (EE). The outcomes portray a compelling narrative—both IoT fairness and RB fairness exhibit upward trajectories as the cohort of associated devices expands. Moreover, the energy efficiency (EE) metric demonstrates a consistent ascent as user numbers increase. However, a noteworthy corollary emerges: EE encounters a dip as Quality of Service (QoS) rate requirements surge.

References

[1] C. V. Networking, "Cisco global cloud index: Forecast and methodology, 2016–2021," *White paper. Cisco Public, San Jose*, vol. 1, 2016.

[2] M. H. Kashani, M. Madanipour, M. Nikravan, P. Asghari, and E. Mahdipour, "A systematic review of iot in healthcare: Applications, techniques, and trends," *Journal of Network and Computer Applications*, vol. 192, p. 103164, 2021.

[3] B. Guo, D. Zhang, Z. Wang, Z. Yu, and X. Zhou, "Opportunistic iot: Exploring the harmonious interaction between human and the internet of things," *Journal of Network and Computer Applications*, vol. 36, no. 6, pp. 1531–1539, 2013.

[4] P. Zhou, K. Shen, N. Kumar, Y. Zhang, M. M. Hassan, and K. Hwang, "Communication-efficient offloading for mobile-edge computing in 5g heterogeneous networks," *IEEE Internet of Things Journal*, vol. 8, no. 13, pp. 10 237–10 247, 2020.

[5] U. Ghafoor, M. Ali, H. Z. Khan, A. M. Siddiqui, and M. Naeem, "Throughput maximization in hybrid noma assisted beyond 5g heterogeneous networks," in *2021 International Wireless Communications and Mobile Computing (IWCMC)*. IEEE, 2021, pp. 991–996.

[6] R. C. Poonia and L. Raja, "On-demand routing protocols for vehicular cloud computing," in *Research Anthology on Architectures, Frameworks, and Integration Strategies for Distributed and Cloud Computing*. IGI Global, 2021, pp. 96–122.

[7] N. Javaid, A. Sher, H. Nasir, and N. Guizani, "Intelligence in iot-based 5g networks: Opportunities and challenges," *IEEE Communications Magazine*, vol. 56, no. 10, pp. 94–100, 2018.

[8] U. Ghafoor, H. Z. Khan, M. Ali, A. M. Siddiqui, M. Naeem, and I. Rashid, "Energy efficient resource allocation for h-noma assisted b5g hetnets," *IEEE Access*, vol. 10, pp. 91 699–91 711, 2022.

[9] F. F. Qureshi, R. Iqbal, and M. N. Asghar, "Energy efficient wireless communication technique based on cognitive radio for internet of things," *Journal of Network and Computer Applications*, vol. 89, pp. 14–25, 2017.

[10] H. S. Lee, P. Arestis, S. C. Chong, S. Yap, and B. K. Sia, "The heterogeneous effects of urbanisation and institutional quality on greenhouse gas emissions in belt and road initiative countries," *Environmental Science and Pollution Research*, vol. 29, pp. 1087–1105, 2022.

[11] M. AbuNaser and A. A. Alkhatib, "Advanced survey of blockchain for the internet of things smart home," in *2019 IEEE Jordan international joint conference on electrical engineering and information technology (JEEIT)*. IEEE, 2019, pp. 58–62.

[12] H. A. Khattak, H. Arshad, G. Ahmed, S. Jabbar, A. M. Sharif, S. Khalid *et al.*, "Utilization and load balancing in fog servers for health applications," *EURASIP Journal on Wireless Communications and Networking*, vol. 2019, no. 1, pp. 1–12, 2019.

[13] W. N. Edelstein, S. N. Madsen, A. Moussessian, and C. Chen, "Concepts and technologies for synthetic aperture radar from meo and geosynchronous orbits," in *Enabling Sensor and Platform Technologies for Spaceborne Remote Sensing*, vol. 5659. SPIE, 2005, pp. 195–203.

[14] B. Li, Z. Fei, C. Zhou, and Y. Zhang, "Physical-layer security in space information networks: A survey," *IEEE Internet of things journal*, vol. 7, no. 1, pp. 33–52, 2019.

[15] M. T. Knopp, A. Spoerl, M. Gnat, G. Rossmanith, F. Huber, C. Fuchs, and D. Giggenbach, "Towards the utilization of optical ground-to-space links for low earth orbiting spacecraft," *Acta Astronautica*, vol. 166, pp. 147–155, 2020.

[16] S. A. AlQahtani and W. A. Alhomiqani, "A multi-stage analysis of network slicing architecture for 5g mobile networks," *Telecommunication Systems*, vol. 73, pp. 205–221, 2020.

[17] V. Yasin, A. R. Nugraha, M. Zarlis, and I. Junaedi, "Smart system of fast internet access development using backbone network method," *JISICOM (Journal of Information System, Informatics and Computing)*, vol. 2, no. 2, pp. 26–34, 2018.

[18] E. Zeydan and Y. Turk, "On the impact of satellite communications over mobile networks: An experimental analysis," *IEEE Transactions on Vehicular Technology*, vol. 68, no. 11, pp. 11 146–11 157, 2019.

[19] S. Wang, L. Ma, and X. Wang, "Optimization of energy efficiency for uplink wireless information and downlink power transfer system with imperfect csi," *Wireless Communications and Mobile Computing*, vol. 2021, 2021.

[20] M. R. Palattella, J. O'Sullivan, D. Pradas, K. McDonnell, I. Rodriguez, and G. Karagiannis, "5g smart connectivity platform for ubiquitous and automated innovative services," in *2021 IEEE 32nd Annual International Symposium on Personal, Indoor and Mobile Radio Communications (PIMRC)*. IEEE, 2021, pp. 1582–1588.

[21] X. Ding, Z. Ren, H. Lu, and G. Zhang, "Improving sinr via joint beam and power management for geo and leo spectrum-sharing satellite communication systems," *China Communications*, vol. 19, no. 7, pp. 25–36, 2022.

[22] R. Ge, J. Cheng, K. An, and G. Zheng, "Non-orthogonal multiple access enabled two-layer geo/leo satellite network," in *2021 29th European Signal Processing Conference (EUSIPCO)*. IEEE, 2021, pp. 890–894.

[23] T. Leng, P. Duan, D. Hu, G. Cui, and W. Wang, "Cooperative user association and resource allocation for task offloading in hybrid geo-leo satellite networks," *International Journal of Satellite Communications and Networking*, vol. 40, no. 3, pp. 230–243, 2022.

[24] S. H. Chae, S.-W. Jeon, and C. Jeong, "Efficient resource allocation for iot cellular networks in the presence of inter-band interference," *IEEE Transactions on Communications*, vol. 67, no. 6, pp. 4299–4308, 2019.

[25] M. Grillo, A. A. Dowhuszko, M.-A. Khalighi, and J. Hämäläinen, "Resource allocation in a quantum key distribution network with leo and geo trusted-repeaters," in *2021 17th International Symposium on Wireless Communication Systems (ISWCS)*. IEEE, 2021, pp. 1–6.

[26] O. Karatalay, I. Psaromiligkos, and B. Champagne, "Energy-efficient resource allocation for d2d-assisted fog computing," *IEEE Transactions on Green Communications and Networking*, 2022.

[27] N. Moghaddas-Gholian, V. Solouk, and H. Kalbkhani, "Relay selection and power allocation for energy-load efficient network-coded cooperative unicast d2d communications," *Peer-to-Peer Networking and Applications*, vol. 15, no. 2, pp. 1281–1293, 2022.

[28] K. Wang, W. Chen, J. Li, Y. Yang, and L. Hanzo, "Joint task offloading and caching for massive mimo-aided multi-tier computing networks," *IEEE Transactions on Communications*, vol. 70, no. 3, pp. 1820–1833, 2022.

[29] S. Mao, S. He, and J. Wu, "Joint uav position optimization and resource scheduling in space-air-ground integrated networks with mixed cloud-edge computing," *IEEE Systems Journal*, vol. 15, no. 3, pp. 3992–4002, 2020.

[30] R. Basir, S. Qaisar, M. Ali, M. Naeem, and A. Anpalagan, "Energy efficient resource allocation in cache-enabled fog networks," *Transactions on Emerging Telecommunications Technologies*, vol. 32, no. 11, p. e4343, 2021.

[31] R. Basir, S. Qaisar, M. Ali, and M. Naeem, "Cloudlet selection in cache-enabled fog networks for latency sensitive iot applications," *IEEE Access*, vol. 9, pp. 93 224–93 236, 2021.

[32] R. Basir, S. B. Qaisar, M. Ali, M. Naeem, K. C. Joshi, and J. Rodriguez, "Latency-aware resource allocation in green fog networks for industrial iot applications," in *2020 IEEE International Conference on Communications Workshops (ICC Workshops)*. IEEE, 2020, pp. 1–6.

[33] R. K. Jain, D.-M. W. Chiu, W. R. Hawe *et al.*, "A quantitative measure of fairness and discrimination," *Eastern Research Laboratory, Digital Equipment Corporation, Hudson, MA*, vol. 21, 1984.

[34] B. Di, H. Zhang, L. Song, Y. Li, and G. Y. Li, "Ultra-dense leo: Integrating terrestrial-satellite networks into 5g and beyond for data offloading," *IEEE Transactions on Wireless Communications*, vol. 18, no. 1, pp. 47–62, 2018.

[35] D. Zhou, M. Sheng, R. Liu, Y. Wang, and J. Li, "Channel-aware mission scheduling in broadband data relay satellite networks," *IEEE Journal on Selected Areas in Communications*, vol. 36, no. 5, pp. 1052–1064, 2018.

[36] H. Bian and R. Liu, "Reliable and energy-efficient leo satellite communication with ir-harq via power allocation," *Sensors*, vol. 22, no. 8, p. 3035, 2022.

[37] J. F. O'Hara and D. R. Grischkowsky, "Comment on the veracity of the itu-r recommendation for atmospheric attenuation at terahertz frequencies," *IEEE Transactions on Terahertz Science and Technology*, vol. 8, no. 3, pp. 372–375, 2018.

[38] L. Tang, X. Zhang, H. Xiang, Y. Sun, and M. Peng, "Joint resource allocation and caching placement for network slicing in fog radio access networks," in *2017 IEEE 18th International Workshop on Signal Processing Advances in Wireless Communications (SPAWC)*. IEEE, 2017, pp. 1–6.

[39] A. Mohajer, M. S. Daliri, A. Mirzaei, A. Ziaeddini, M. Nabipour, and M. Bavaghar, "Heterogeneous computational resource allocation for noma: Toward green mobile edge-computing systems," *IEEE Transactions on Services Computing*, 2022.

[40] A. Charnes and W. W. Cooper, "Programming with linear fractional functionals," *Naval Research logistics quarterly*, vol. 9, no. 3-4, pp. 181–186, 1962.

[41] M. Hong and Z.-Q. Luo, "Distributed linear precoder optimization and base station selection for an uplink heterogeneous network," *IEEE transactions on signal processing*, vol. 61, no. 12, pp. 3214–3228, 2013.

[42] M. A. Duran and I. E. Grossmann, "An outer-approximation algorithm for a class of mixed-integer nonlinear programs," *Mathematical programming*, vol. 36, no. 3, pp. 307–339, 1986.

[43] R. Fletcher and S. Leyffer, "Solving mixed integer nonlinear programs by outer approximation," *Mathematical programming*, vol. 66, no. 1-3, pp. 327–349, 1994.

[44] A. H. Land and A. G. Doig, "An automatic method of solving discrete programming problems," *Econometrica: Journal of the Econometric Society*, pp. 497–520, 1960.

[45] C. A. Floudas and P. M. Pardalos, *Encyclopedia of optimization*. Springer Science & Business Media, 2001, vol. 1.

[46] C. A. Floudas, *Nonlinear and mixed-integer optimization: fundamentals and applications*. Oxford University Press, 1995.

[47] C. F. Van Loan and G. H. Golub, *Matrix computations*. Johns Hopkins University Press, 1983.

Author Biography

Muhammad Abdullah is currently pursuing a Master of Science (M.S.) degree in Electrical (Telecommunication) Engineering from the National University of Sciences and Technology (NUST), Pakistan. He earned his Bachelor of Engineering (B.E.) degree in Telecommunication Engineering from the University of Engineering and Technology (Taxila), Pakistan, in 2021. His research interests encompass a wide range of areas, such as metamaterials, resource allocation, as well as spectrum and energy efficiency in wireless communication systems.

Humayun Zubair Khan (M'19, SM'22) is doing postdoctoral research at University of Glasgow, UK. He received degree of PhD in Electrical (Telecommunication) Engineering from Military College of Signals (MCS), National University of Sciences and Technology (NUST), Pakistan in 2020. He received his B.E and M.S. degree in Electrical (Telecommunication) Engineering from National University of Sciences and Technology (NUST), Pakistan in the year 2006 and 2013 respectively. He received Master of Business Administration degree with majors in Finance from Virtual University of Pakistan in 2011. He was a recipient of the Indigenous Ph.D. Fellowship program scholarship. His research interests include resource allocation, optimization, & metasurfaces in 5G/ 6G wireless communications.

Umair Fakhar is pursuing M.S. degree in Electrical (Telecommunication) Engineering from National University of Sciences and Technology (NUST), Pakistan. He received his B.E degree in Electrical (Telecommunication) Engineering from National University of Sciences and Technology (NUST), Pakistan in the year 2015. His research interests include resource allocation, spectrum and energy efficiency in wireless communication systems. .

Ahmad Naeem Akhtar is PhD in Telecommunications Engineering from NUST Pakistan. He has been associated with research and academia for almost more than a decade. Besides, he has worked in Telecommunication Engineering field for more than 15 years. At present, he is doing as Dir IT and HoD IT Department (Academics) in Lahore Garrison university. His research interests include Software Defined Networks, IT Data Center virtualization, IoT and Algorithm Analysis.

Shuja Ansari (M'15, SM'20) is a Lecturer in Autonomous Systems and Connectivity at James Watt School of Engineering of University of Glasgow (UofG). He received his MSc with distinction and PhD in Engineering from Glasgow Caledonian University in 2015 and 2019, respectively. He is a Chartered Engineering who has a strong background with over a decade of experience in telecommunications. He is the 5G and IoT use case lead for the Wave-1 Urban 5G project funded by the Scotland 5G Centre and project manager for Glasgow COMPORAN funded by DSIT. His research interests include wireless communications, systems integration, terrestrial/airborne mobile networks, security and privacy in communications and Internet of Things (IoT).

Declaration of interests

☒ The authors declare that they have no known competing financial interests or personal relationships that could have appeared to influence the work reported in this paper.

☐The authors declare the following financial interests/personal relationships which may be considered as potential competing interests: